MIKE Powered by DHI

MIKE 21

Spectral Wave Module

Scientific Documentation

DHI headquarters
Agern Allé 5
DK-2970 Hørsholm
Denmark

+45 4516 9200 Telephone
+45 4516 9333 Support
+45 4516 9292 Telefax

mike@dhigroup.com
www.mikepoweredbydhi.com

PLEASE NOTE

CONTENTS

MIKE 21
Spectral Wave Module
Scientific Documentation

APPENDICES

1 Introduction

MIKE 21 SW is a new generation spectral wind-wave model based on unstructured meshes. The model simulates the growth, decay and transformation of wind-generated waves and swell waves in offshore and coastal areas.

Figure 1.1 MIKE 21 SW is a state-of-the-art numerical tool for prediction and analysis of wave climates in offshore and coastal areas

MIKE 21 SW includes two different formulations:

- Directional decoupled parametric formulation
- Fully spectral formulation

The directional decoupled parametric formulation is based on a parameterization of the wave action conservation equation. The parameterization is made in the frequency domain by introducing the zeroth and first moment of the wave action spectrum as dependent variables following Holthuijsen (1989).

The fully spectral formulation is based on the wave action conservation equation, as described in e.g. Komen et al (1994) and Young (1999), where the directional-frequency wave action spectrum is the dependent variable.

The basic conservation equations are formulated in either Cartesian coordinates for small-scale applications or polar spherical coordinates for large-scale applications.

MIKE 21 SW includes the following physical phenomena:

- Wave growth by action of wind
- Non-linear wave-wave interaction
- Dissipation due to white-capping
- Dissipation due to bottom friction
- Dissipation due to depth-induced wave breaking
- Refraction and shoaling due to depth variations
- Wave-current interaction
- Effect of time-varying water depth

The discretisation of the governing equation in geographical and spectral space is performed using cell-centred finite volume method. In the geographical domain, an unstructured mesh technique is used. The time integration is performed using a fractional step approach where a multi-sequence explicit method is applied for the propagation of wave action.

2 Application Areas

MIKE 21 SW is used for the assessment of wave climates in offshore and coastal areas - in hindcast and forecast mode.

A major application area is the design of offshore, coastal and port structures where accurate assessment of wave loads is of utmost importance to the safe and economic design of these structures. Measured data is often not available during periods long enough to allow for the establishment of sufficiently accurate estimates of extreme sea states. In this case, the measured data can then be supplemented with hindcast data through the simulation of wave conditions during historical storms using MIKE 21 SW.

MIKE 21 SW is particularly applicable for simultaneous wave prediction and analysis on regional scale (like the North Sea, see Figure 2.1) and local scale (west coast of Jutland, Denmark, see Figure 2.3). Coarse spatial and temporal resolution is used for the regional part of the mesh and a high-resolution boundary- and depth-adaptive mesh is describing the shallow water environment at the coastline.

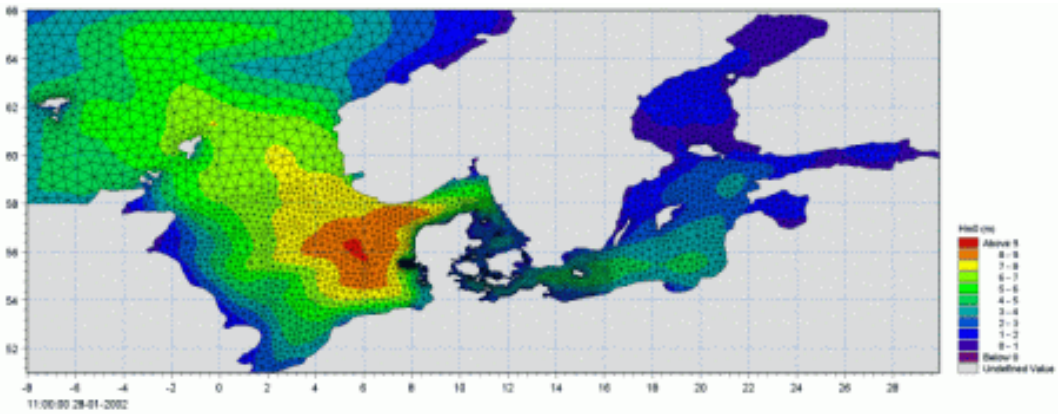

Figure 2.1 A MIKE 21 SW forecast application in the North Sea and Baltic Sea. The chart shows a wave field illustrated by the significant wave height in top of the computational mesh

MIKE 21 SW is also used in connection with the calculation of the sediment transport, which for a large part is determined by wave conditions and associated wave-induced currents. The wave-induced current is generated by the gradients in radiation stresses that occur in the surf zone. MIKE 21 SW can be used to calculate the wave conditions and associated radiation stresses.

Figure 2.2 Illustration of typical application areas

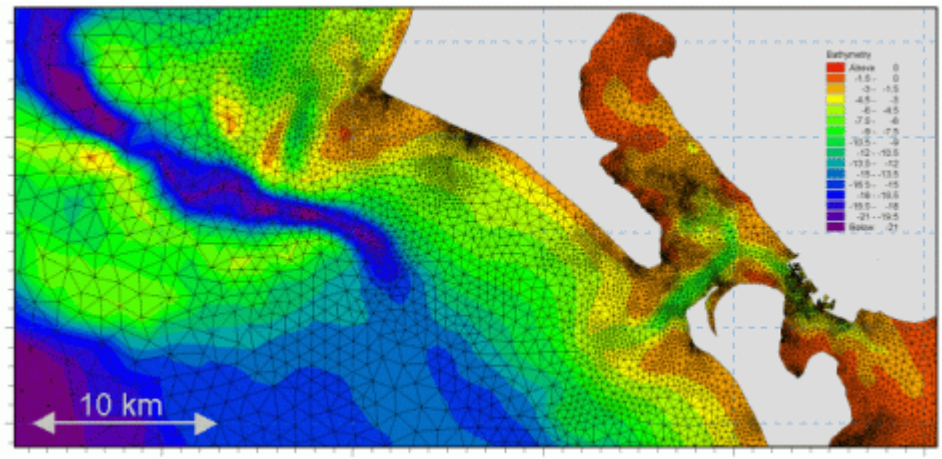

Figure 2.3 Example of a computational mesh used for transformation of offshore wave statistics using the directionally decoupled parametric formulation

MIKE 21 SW can also be applied on global scale as illustrated in Figure 2.4.

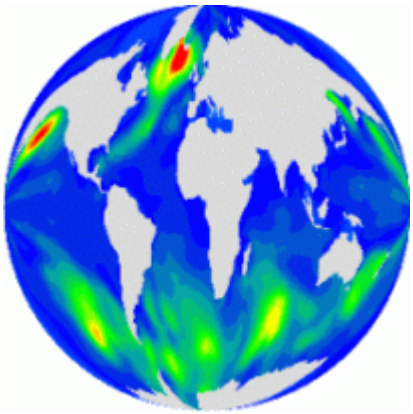

Figure 2.4 Example of a global application of MIKE 21 SW. Results from such a model can be used as boundary conditions for regional scale forecast or hindcast models

3 Basic Equations

3.1 General

The dynamics of the gravity waves are described by the transport equation for wave action density. For small-scale applications the basic transport is usually formulated in Cartesian coordinates, while spherical polar coordinates are used for large-scale applications. The wave action density spectrum varies in time and space and is a function of two wave phase parameters. The two wave phase parameters can be the wave number vector $\vec{k}$ with magnitude, k, and direction, θ. Alternatively, the wave phase parameters can also be the wave direction, θ, and either the relative (intrinsic) angular frequency, $\sigma = 2\pi f_r$, or the absolute angular frequency, $\omega = 2\pi f_a$. In the present model a formulation in terms of the wave direction, θ, and the relative angular frequency, σ, has been chosen. The action density, $N(\sigma,\theta)$, is related to the energy density $E(\sigma,\theta)$ by

$$N = \frac{E}{\sigma} \tag{3.1}$$

For wave propagation over slowly varying depths and currents the relation between the relative angular frequency (as observed in a frame of reference moving with the current velocity) and the absolute angular frequency, ω, (as observed in a fixed frame) is given by the linear dispersion relation

$$\sigma = \sqrt{gk\tanh(kd)} = \omega - \vec{k}\cdot\vec{U} \tag{3.2}$$

where g is the acceleration of gravity, d is the water depth and $\vec{U}$ is the current velocity vector. The magnitude of the group velocity, c_g, of the wave energy relative to the current is given by

$$c_g = \frac{\partial\sigma}{\partial k} = \frac{1}{2}\left(1 + \frac{2kd}{\sinh(2kd)}\right)\frac{\sigma}{k} \tag{3.3}$$

The phase velocity, c, of the wave relative to the current is given by

$$c = \frac{\sigma}{k} \tag{3.4}$$

The frequency spectrum is limited to the range between a minimum frequency, $\sigma_{\min}$, and a maximum frequency, $\sigma_{\max}$. The frequency spectrum is split up into a deterministic prognostic part for frequencies lower than a cut-off frequency and an analytical diagnostic part for frequencies higher than the cut-off frequency. A dynamic cut-off frequency depending on the local wind speed and the mean frequency is used as in the WAM Cycle 4 model (see WAMDI Group (1988) and Komen et al. (1994)). The deterministic part of the spectrum is determined solving the transport equation for wave action density using numerical methods. Above the cut-off frequency limit of the prognostic region, a parametric tail is applied

$$E(\sigma,\theta) = E(\sigma_{\max},\theta)\left(\frac{\sigma}{\sigma_{\max}}\right)^{-m} \tag{3.5}$$

where *m* is a constant. In the present model *m* = 5 is applied. The maximum prognostic frequency is determined as

$$\sigma_{cut-off} = \min\left[\sigma_{\max}, \max(2.5\bar{\sigma}, 4\sigma_{PM})\right] \tag{3.6}$$

where $\sigma_{\max}$ is the maximum discrete frequency used in the deterministic wave model, $\bar{\sigma}$ is the mean relative frequency and $\sigma_{PM} = g/(28u_{10})$ is the Pierson-Moskowitz peak frequency for fully developed waves (U_{10} is the wind speed at 10 m above the mean sea level) The diagnostic tail is used in the calculation of the non-linear transfer and in the calculation of the integral parameters used in the source functions. Below the minimum frequency the spectral densities is assumed to be zero.

As standard the mean frequency, used in Eq. (3.6), is calculated based on the whole spectrum. For swell dominated wave conditions this can result in a too low cut-off frequency and thereby an underestimation of the local generated wind waves. The predictions can be improved by calculation the mean frequency based on only the wind-sea part of the spectrum. The separation of wind-sea and swell can be estimated using the definitions in Section 5.1.

3.2 Wave Action Conservation Equations

The governing equation is the wave action balance equation formulated in either Cartesian of spherical coordinates (see Komen et al. (1994) and Young (1999)).

Cartesian coordinates

In horizontal Cartesian coordinates, the conservation equation for wave action can be written as

$$\frac{\partial N}{\partial t} + \nabla\cdot(\vec{v}N) = \frac{S}{\sigma} \tag{3.7}$$

where $N(\vec{x},\sigma,\theta,t)$ is the action density, *t* is the time, $\vec{x} = (x, y)$ is the Cartesian coordinates, $\vec{v} = (c_x, c_y, c_\sigma, c_\theta)$ is the propagation velocity of a wave group in the four-dimensional phase space $\vec{x}$, σ and θ, and *S* is the source term for the energy balance equation. ∇ is the four-dimensional differential operator in the $\vec{x}$, σ, θ-space. The four characteristic propagation speeds are given by

$$(c_x, c_y) = \frac{d\vec{x}}{dt} = \vec{c}_g + \vec{U} \tag{3.8}$$

$$c_\sigma = \frac{d\sigma}{dt} = \frac{\partial\sigma}{\partial d}\left[\frac{\partial d}{\partial t} + \vec{U}\cdot\nabla_{\vec{x}} d\right] - c_g\vec{k}\cdot\frac{\partial\vec{U}}{\partial s} \tag{3.9}$$

$$c_\theta = \frac{d\theta}{dt} = -\frac{1}{k}\left[\frac{\partial\sigma}{\partial d}\frac{\partial d}{\partial m} + \vec{k}\cdot\frac{\partial\vec{U}}{\partial m}\right] \tag{3.10}$$

Here, *s* is the space coordinate in wave direction θ, and *m* is a coordinate perpendicular to *s*. $\nabla_{\vec{x}}$ is the two-dimensional differential operator in the $\vec{x}$-space.

Spherical coordinates

In spherical coordinates, the conserved property is the action density $\hat{N}(\vec{x},\sigma,\theta,t)$. Here, $\vec{x} = (\phi,\lambda)$ is the spherical coordinates, where ϕ is the latitude and λ is the longitude. The action density $\hat{N}$ is related to the normal action density *N* (and normal energy density E) through $\hat{N}d\sigma d\theta d\phi d\lambda = Nd\sigma d\theta dxdy$, or

$$\hat{N} = NR^2\cos\phi = \frac{ER^2\cos\phi}{\sigma} \tag{3.11}$$

where *R* is the radius of the earth. In spherical polar coordinates the wave action balance equation can be written

$$\frac{\partial\hat{N}}{\partial t} + \frac{\partial}{\partial\phi}c_\phi\hat{N} + \frac{\partial}{\partial\lambda}c_\lambda\hat{N} + \frac{\partial}{\partial\sigma}c_\sigma\hat{N} + \frac{\partial}{\partial\theta}c_\theta\hat{N} = \frac{\hat{S}}{\sigma} \tag{3.12}$$

Here $\hat{S}(\vec{x},\sigma,\theta,t) = SR^2\cos\phi$ is the total source and sink function. The four characteristic propagation speeds are given by

$$c_\phi = \frac{d\phi}{dt} = \frac{c_g\cos\theta + u_\phi}{R} \tag{3.13}$$

$$c_\lambda = \frac{d\lambda}{dt} = \frac{c_g\sin\theta + u_\lambda}{R\cos\phi} \tag{3.14}$$

$$\begin{aligned} c_\sigma = \frac{d\sigma}{dt} &= \frac{\partial\sigma}{\partial d}\left[\frac{\partial d}{\partial t} - \frac{d}{R}\left(\frac{1}{\cos\phi}\frac{du_\lambda}{\partial\lambda} + \frac{du_\phi}{\partial\phi} - u_\phi\tan\phi\right)\right] \\ &- \frac{kc_g}{R}\left[\begin{array}{l}\cos\theta\left(\sin\theta\frac{du_\lambda}{d\phi} + \cos\theta\frac{du_\phi}{d\phi}\right) + \frac{\sin\theta}{\cos\phi}\left(\sin\theta\frac{du_\lambda}{d\lambda} + \cos\theta\frac{du_\phi}{d\lambda}\right) - \\ \cos\theta\tan\phi\left(u_\lambda\sin\phi + u_\phi\cos\theta\right)\end{array}\right] \end{aligned} \tag{3.15}$$

$$\begin{aligned} c_\theta = \frac{d\theta}{dt} &= \frac{c_g\sin\theta\tan\phi}{R} + \frac{1}{Rk}\frac{\partial\sigma}{\partial d}\left(\sin\theta\frac{\partial d}{\partial\phi} - \frac{\cos\theta}{\cos\phi}\frac{\partial d}{\partial\lambda}\right) + \\ &\frac{\sin\theta}{R}\left(\sin\theta\frac{\partial u_\lambda}{\partial\phi} + \cos\theta\frac{\partial u_\phi}{\partial\phi}\right) - \frac{\cos\theta}{R\cos\phi}\left(\sin\theta\frac{\partial u_\lambda}{\partial\lambda} + \cos\theta\frac{\partial u_\phi}{\partial\lambda}\right) \end{aligned} \tag{3.16}$$

Here (u_ϕ, u_λ) are the components of the depth-averaged current $\vec{U}$ in the geographical space. For the wave direction θ a nautical convention is used (positive clockwise from true North): the direction from where the wind is blowing.

3.3 Source Functions

The energy source term, S, represents the superposition of source functions describing various physical phenomena

$$S = S_{in} + S_{n1} + S_{ds} + S_{bot} + S_{surf} \tag{3.17}$$

Here S_{in} represents the generation of energy by wind, S_{nl} is the wave energy transfer due non-linear wave-wave interaction, S_{ds} is the dissipation of wave energy due to whitecapping, S_{bot} is the dissipation due to bottom friction and S_{surf} is the dissipation of wave energy due to depth-induced breaking.

3.3.1 Wind input

In a series of studies by Janssen (1989), Janssen et al. (1989) and Janssen (1991), it is shown that the growth rate of the waves generated by wind depends also on the wave age. This is because of the dependence of the aerodynamic drag on the sea state.

The input source term, S_{in} is given by

$$S_{in}(f,\theta) = \max(\alpha, \gamma E(f,\theta)) \tag{3.18}$$

where α is the linear growth and γ is the nonlinear growth rate.

Non-linear growth

A simple parameterisation of the growth rate, γ ,of the waves is obtained by Janssen (1991) by fitting a curve to his earlier detailed numerical results. This fitted curve compares favourably with observations by Snyder et al., 1981. Janssen suggested

$$\gamma = \varepsilon \beta \sigma x^2 \tag{3.19}$$

where ε is the ratio of density of air to water ρ_a / ρ_w and σ is the relative circular frequency. x is given by

$$x = \frac{u_*}{c}\cos(\theta - \theta_w) \tag{3.20}$$

where u_* is the wind friction velocity, c is the phase speed and θ and θ_w are the wave and wind directions, respectively. Finally, β is given by:

$$\beta = \frac{1.2}{\kappa^2}\mu \ln^4 \mu \qquad \mu \le 1$$
$$\beta = 0 \qquad \mu > 1 \tag{3.21}$$

where κ is von Karman's constant κ=0.41 and μ is the dimensionless critical height

$$\mu = kz_c \tag{3.22}$$

Here k is the wave number and z_c is the critical height defined as the elevation above sea level where the wind speed is exactly equal to the phase speed. Assuming a logarithmic wind profile, the critical height can be written as

$$z_c = z_o \exp(\kappa / x) \tag{3.23}$$

In the actual implementation of WAM, Eq. (3.20) was modified as follows:

$$x = \left(\frac{u_*}{c} + z_\alpha\right)\cos(\theta - \theta_w) \tag{3.24}$$

where $z_\alpha = 0.011$. According to Peter Janssen (private communication, 1995), this was necessary to account for gustiness and obtain a reasonable growth rate with WAM.

Using Eqs. (3.21) - (3.24), the growth rate due to wind input can be calculated as

$$\gamma = \left(\frac{\rho_a}{\rho_w}\right)\left(\frac{1.2}{\kappa^2}\mu \ln^4 \mu\right)\sigma\left[\left(\frac{u_*}{c} + z_\alpha\right)\cos(\theta - \theta_w)\right]^2 \qquad \mu \le 1$$
$$\gamma = 0 \qquad \mu > 1 \tag{3.25}$$

where

$$\mu = kz_o \exp(\kappa / x) \tag{3.26}$$

For a given wind speed and direction, the growth rate of waves of a given frequency and direction depends on the friction velocity, u_* and sea roughness, z_o. In order to calculate u_*, Janssen assumed a logarithmic profile for the wind speed *u(z)* of the form

$$u(z) = \frac{u_*}{\kappa}\ln\left(\frac{z + z_{ow}}{z_{ob} + z_{ow}}\right) \qquad z_0 = z_{ob} + z_{ow} \tag{3.27}$$

where z_{ob} models the effect of gravity-capillary waves (can be seen as background roughness) and z_{ow} models the effect of short gravity waves. z_{ob} is parameterised as

$$z_{0b} = z_{Charnock} u_*^2 / g \tag{3.28}$$

where $z_{Charnock}$ is the Charnock parameter. The default value are $z_{Charnock} = 0.01$. Usually, $z >> z_{ow}$ and in that case

$$u_* = \frac{\kappa u(z)}{\ln\left(\frac{z}{z_0}\right)} \tag{3.29}$$

Three different formulations for estimating u_* and z_c has been implemented in the model:

Uncoupled model using a drag law

Here the relation between the wind speed $U_w = u(z)$ at a level $z = z_{wind}$ and the wind friction velocity is given by a simple empirical formulation

$$u_*^2 = C_D \cdot U_w^2, C_D = \alpha_{drag} + \beta_{drag} \cdot U_w \tag{3.30}$$

where α_{drag} and β_{drag} are two constants. The default values are $z_{wind} = 10\ m$, $\alpha_{drag} = 6.3 \cdot 10^{-4}$ and $\beta_{drag} = 6.6 \cdot 10^{-5}$, cf. Smith & Banke (1975). Then the sea roughness is obtained using Eq. (3.29).

$$z_0 = z_{wind} \exp\left(-\frac{\kappa U_w}{u_*}\right) \tag{3.31}$$

Uncoupled model using Charnock

If z_{ow} is assumed to be small compared to z_{ob}, the air roughness is given by

$$z_0 = z_{0b} = z_{charnock} u_*^2 / g \tag{3.32}$$

For a given wind speed $U_w = u(z)$ at a level $z = z_{wind}$ it is possible to solve by Eq. (3.29) and (3.32) iteratively to obtain the roughness length z_0 and the friction velocity u_*. Now, to limit the number of repetitive calculations of this type, the values of τ for various combinations of U_w can be pre-computed and stored. The range of U_w used is: 0-50 m/s in steps of 0.5 m/s.

Coupled model

Here the sea roughness is given by

$$z_o = z_{ob} + z_{ow} = z_{ob}\left(1 - \frac{\tau_w}{\tau}\right)^{-½} = \frac{z_{charnock} u_*^2}{g}\left(1 - \frac{\tau_w}{\rho_{air} u_*^2}\right)^{-½} \tag{3.33}$$

where τ_w is the wave induced stress, and τ is the total stress $\tau = \rho_{air} u_*^2$. For a given wind speed $U_w = u(z)$ at a level $z = z_{wind}$ and the wave induced stress, it is possible to solve Eqs. (3.29) and (3.33) iteratively to obtain u_*. To limit the number of repetitive calculations of this type, the values of τ for various combinations of u_{10} and τ_w can be pre-computed and stored. The range of U_{10} used is: 0-50 m/s in steps of 0.5 m/s, while the range of τ_ω is: 0-5 m^2/s^2 in steps of 0.05 m^2/s^2.

The wave-induced stress, τ_w is calculated as follows

$$\tau_w = \int \left. \frac{\partial \vec{P}}{\partial t} \right|_{wind} df\, d\theta \tag{3.34}$$

where $\vec{P}$ is the wave momentum given by

$$\vec{P} = \rho_w \sigma E(f,\theta)\vec{\imath} \tag{3.35}$$

Here $\vec{\imath}$ is the unit vector along the wave direction ($\vec{\imath} = \vec{k}/k$). From Eq. (3.18) we obtain

$$\frac{\partial \vec{P}}{\partial t} = \rho_w \sigma \left. \frac{\partial E}{\partial t} \right|_{wind} \vec{\imath} = \rho_w \sigma \gamma F \vec{\imath} \tag{3.36}$$

where γ is the growth rate of the waves due to wind. Splitting the integral into low and high frequency parts, one obtains

$$\vec{\tau}_w = \vec{\tau}_{w,prognostic} + \vec{\tau}_{w,diagnostic} \tag{3.37}$$

where

$$\vec{\tau}_{w,prognostic} = \int_o^{f_{\max}} \int_\theta \rho_w \gamma E 2\pi f\, df\, d\theta \vec{l} \tag{3.38}$$

$$\vec{\tau}_{w,diagnostic} = \int_{f_{\max}}^{\infty} \int_\theta \rho_w \gamma E 2\pi f\, df\, d\theta \vec{l} \tag{3.39}$$

Here $f_{\max}$ is the maximum prognostic frequency.

The prognostic part $\vec{\tau}_{w,prognostic}$ is calculated by numerical integration of Eq. (3.38) using the computed discrete spectra. The diagnostic part $\vec{\tau}_{w,diagnostic}$ (containing the high frequency part of the spectrum) is calculated assuming a f^{-5} spectra shape, see Eq. (3.5). For this high frequency waves, the wave celerity can be evaluated using the expression for deep water waves. Thus, $c = g/2\pi f$. Now, substituting Eq. (3.5) with m=5 and Eq. (3.25) into Eq. (3.39), we obtain:

$$\vec{\tau}_{w,diagnostic} = \frac{(2\pi)^4}{g^2} \cdot f_{\max}^5 \cdot \rho_a u_*^2 \int_\theta E(f_{\max,\theta}) \cos^2(\theta - \varphi) \cdot I_{\tau_w} d\theta \vec{l} \tag{3.40}$$

where

$$I_{\tau_w} = \int_{f_{\max}}^{\infty} \beta \frac{df}{f} \tag{3.41}$$

By changing the variable f in Eq. (3.41) to a new variable y (defined as the square root of dimensionless roughness, $\sqrt{kz_o}$)

$$y = 2\pi f \sqrt{z_o / g} \tag{3.42}$$

Eq. (3.41) is rewritten as

$$I_{\tau_\omega} = \int_{y_{\max}}^{1} \beta \frac{dy}{y} \tag{3.43}$$

where $y_{\max} = 2\pi f_{\max} \sqrt{z_o / g}$ and the upper limit is set to 1.0. Assuming z_{ch} = 0.0185, this upper limit corresponds to a frequency of about 180 times the Pierson Moskowitz peak frequency.

Eq. (3.43) can be re-written as

$$I_{\tau\omega} = \int_{y_{\max}}^{1} \frac{1.2}{\kappa^2} \mu \ln^4 \mu \frac{dy}{y} \tag{3.44}$$

where

$$\mu = kz_o \exp(\kappa / x) = y^2 \exp(\kappa / x) \tag{3.45}$$

$$x = \left(\frac{u_*}{C} + z_\alpha \right) \cos(\theta - \varphi) = \left(\frac{u_*}{\sqrt{gz_o}} \cdot y + z_\alpha \right) \cos(\theta - \varphi) \tag{3.46}$$

Substituting Eq. (3.46) into Eq. (3.45), we obtain

$$\mu = y^2 \exp\left\{ \frac{\kappa}{\left(\frac{u_*}{\sqrt{gz_o}} \cdot y + z_\alpha \right) \cos(\theta - \varphi)} \right\} \tag{3.47}$$

Now, $\vec{\tau}_{w,diagnostic}$ can be calculated as

$$\vec{\tau}_{w,diagnostic} = \frac{(2\pi)^4}{g^2} \cdot f_{\max}^5 \cdot \rho_a u_*^2 \int_{\theta=\varphi-\pi/2}^{\varphi+\pi/2} E(f_{\max,\theta}) \cos^2(\theta - \varphi) \cdot I_{\tau_w} d\theta \vec{l} \tag{3.48}$$

Where I_{τ_w} is given by Eq. (3.44) and μ is given by Eq. (3.47).

From Eqs. (3.44) and (3.47) it is clear that for given values of z_o, u_* and $(\theta - \theta_w)$, $I_{\tau_w}(z_0, u_*, (\theta - \theta_w))$ can be calculated. To improve the efficiency I_{τ_w} can be precomputed for various values of the dependent parameters, in the same way it was done for τ. Alternatively if $z_o = \alpha u_*^2 / g$, it follows that I_{τ_w} is a function of α, u_* and $(\theta - \varphi)$. Thus, a table may be computed for I_{τ_w} with the following parameter ranges: α goes from 0.01→0.11, step 0.001; u_* goes from 0→5 m/s, step 0.05; $(\theta - \varphi)$ goes from $-\pi/2 \rightarrow \pi/2$, step $\pi/12$.

There are some significant differences between the procedure described above and what is implemented in WAM cycle 4. Basically, WAM approximates Eq. (3.48) as follows:

$$\vec{\tau}_{w,diagnostic} = \frac{(2\pi)^4}{g^2} \cdot f_{\max}^5 \cdot \rho_a u_*^2 \int_{\theta=\varphi-\pi/2}^{\varphi+\pi/2} E(f_{\max,}\theta)\cos^3(\theta-\varphi) \cdot I'_{\tau_w}(\alpha, u_*) d\theta \vec{m} \tag{3.49}$$

where

$$I'_{\tau\omega}(\alpha, u_*) = \int_{y_{\max}}^{1} \frac{1.2}{\kappa^2} \mu' \ln^4 \mu' \frac{dy}{y} \tag{3.50}$$

$$\mu' = y^2 \exp\left\{ \frac{\kappa}{\left(\frac{u_*}{\sqrt{g z_o}} y + z_\alpha \right)} \right\} \tag{3.51}$$

and $\vec{m}$ is the unit vector in the direction of the wind. The omission of the cosine term in Eq. (3.51) appears to be an error (compare Eq. (3.47) and Eq. (3.51)). This error cannot be compensated by the use of $\cos^3$ (Eq. (3.49)) instead of $\cos^2$ (Eq. (3.48)). Furthermore, it is not clear why the direction of $\vec{\tau}_w$ was changed to the wind direction instead of the wave direction. At the time of writing this report, the WAM implementation (Eqs. (3.49) to (3.51)) is used in the present model.

Linear growth

The linear growth, α, is obtained following the approach by Ris (1997)

$$\alpha = \begin{cases} \frac{c}{g^2 2\pi}\left((u_* \cos(\theta - \theta_w))^4\right)\exp\left(-\left(\frac{\sigma}{\sigma_{PM}}\right)^{-4}\right) & \cos(\theta - \theta_w) > 0 \\ 0 & \cos(\theta - \theta_w) \le 0 \end{cases} \quad (3.52)$$

where $c = 1.5 \cdot 10^{-3}$ and the Pierson-Moskowitz peak frequency is defined by

$$\sigma_{PM} = \frac{0.13 g 2\pi}{28 u_*} \quad (3.53)$$

The friction velocity u_* is obtained using SEqs. (3.30). The drag coefficients are given by (see Wu (1982))

$$C_D = \begin{cases} 1.2875 \cdot 10^{-3} & U_w < 7.5\ m/s \\ 0.8 \cdot 10^{-3} + 6.5 \cdot 10^{-5} U_w & U_w \ge 7.5\ m/s \end{cases} \quad (3.54)$$

where U_w is given at $z = 10\ m$.

3.3.2 Quadruplet-wave interactions

The exact computations of the three-dimensional non-linear Boltzmann integral expressions for S_{nl} (Hasselmann, 1962) are too time consuming to be incorporated in a general numerical wave model. Thus, a parameterisation of S_{nl} is required. The discrete interaction approximation (DIA) is the commonly used parameterisation of S_{nl} in third generation wave models. The DIA was developed by S. Hasselmann et al., 1985. The description below is taken from Komen et al., 1994 (pp. 226-228).

S. Hasselmann et al. (1985) constructed a non-linear interaction operator by the superposition of a small number of discrete interaction configurations composed of neighbouring and finite distance interaction combinations. They found that the exact non-linear transfer could be well simulated by just one mirror-image pair of intermediate range interaction configurations. In each configuration, two wave numbers were taken as identical: $\vec{k}_1 = \vec{k}_2 = \vec{k}$, while $\vec{k}_3$ and $\vec{k}_4$ $\left(\neq \vec{k}\right)$ lie at an angle to $\vec{k}$ as required by the resonance condition[1]

The second configuration is obtained from the first by reflecting the wave numbers k_3 and k_4 with respect to the k-axis (see also Figure 3.1). The scale and direction of the reference wave number are allowed to vary continuously in wave number space.

1 Resonance condition requires that $\vec{k}_1 + \vec{k}_2 - \vec{k}_3 - \vec{k}_4 = 0$ and $\omega_1 + \omega_2 - \omega_3 - \omega_4 = 0$.

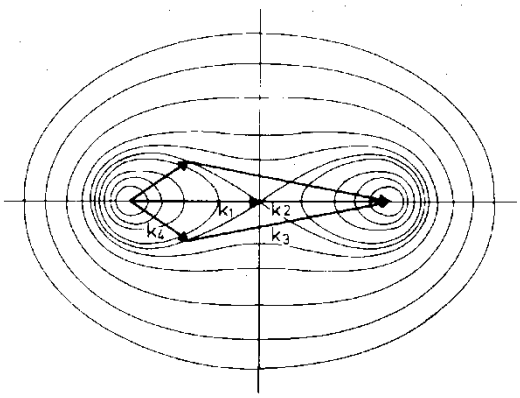

Figure 3.1 The two interaction configurations used in the discrete-interaction approximation. Contour lines represent the possible end points of the vectors k_1 and k_4 for any interaction quadruplet in the full interaction space. (from Komen et al., 1994).

The simplified non-linear operator is computed by applying the same symmetrical integration method as is used to integrate the exact transfer integral (see also Hasselmann and Hasselmann, 1985b), except that the integration is taken over a two-dimensional continuum and two discrete interactions instead of five-dimensional interaction phase space. Just as in the exact case the interactions conserve energy, momentum and action.

For the configurations:

$$\begin{aligned} \omega_1 &= \omega_2 = \omega \\ \omega_3 &= \omega(1+\lambda) = \omega_+ \\ \omega_4 &= \omega(1-\lambda) = \omega_- \end{aligned} \tag{3.55}$$

where $\lambda = 0.25$, satisfactory agreement with the exact computations was achieved. From the resonance conditions the angles θ_3, θ_4 of the wave numbers $k_3(k_+)$ and $k_4(k_-)$ relative to k are found to be θ_3=11.5°, θ_4=-33.6°.

The discrete interaction approximation has its most simple form for the rate of change in time of the action density in wave number space. In agreement with the principle of detailed balance, we have

$$\frac{\partial}{\partial t}\begin{pmatrix} N \\ N_+ \\ N_- \end{pmatrix} = \begin{pmatrix} -2 \\ +1 \\ +1 \end{pmatrix} C g^{-8} f^{-19} \left[N^2 (N_+ + N_-) - 2 N N_+ N_- \right] \Delta k, \tag{3.56}$$

where $\partial N/\partial t, \partial N_+/\partial t, \partial N_-/\partial t$ are the rates of change in action at wave numbers k, k_+, k_- due to the discrete interactions within the infinitesimal interaction phase-space element Δk and *C* is a numerical constant. The net source function S_{nl} is obtained by summing Eq. (3.56) over all wave numbers, directions and interaction configurations.

In terms of the spectral energy densities $E(f_r, \theta)$, the increments to the source functions $S_{nl}(f_r, \theta) (= \partial E / \partial t)$ at the 3 interacting wave numbers are given as: (S. Hasselmann et al., 1985)

$$\begin{Bmatrix} \delta S_{nl} \\ \delta S_{nl+} \\ \delta S_{nl-} \end{Bmatrix} = \begin{Bmatrix} -2\dfrac{\Delta f \Delta\theta}{\Delta f \Delta\theta} \\ (1+\lambda)\dfrac{\Delta f \Delta\theta}{\Delta f_+ \Delta\theta} \\ (1-\lambda)\dfrac{\Delta f \Delta\theta}{\Delta f_- \Delta\theta} \end{Bmatrix} \emptyset(f, E, E_+, E_-) \tag{3.57}$$

where

$$\emptyset(f, F, F_+, F_-) = C' g^{-4} f^{11} \left[E^2 \left(\frac{E_+}{(1+\lambda)^4} + \frac{E_-}{(1-\lambda)^4} \right) - \frac{2EE_+E_-}{(1-\lambda^2)^4} \right] \tag{3.58}$$

where C' is a numerical constant proportional to C, given as 3.10^7, $\Delta f, \Delta f_+ \Delta f_-$ are the discrete spectral resolution at f_r, $f_{r,+}$, *and* $f_{r,-}$, respectively. The increments $\Delta f \Delta\theta$ in the numerator refer to the discrete-interaction phase-space element, while the differentials in the denominator refer to the sizes of the "bins" in which the incremental spectral changes induced by a "collision" are stored. In the above, the angular increments $\Delta\theta$ at $\theta_1, \theta_3, \theta_4$ are taken to be the same, while a possible frequency dependence on Δf is allowed, i.e. $\Delta f_+ \neq \Delta f_- \neq \Delta f$. Eq. (3.57) is summed over all frequencies, directions and interaction configurations to yield the net source function, S_{nl}.

The above analysis is made for deep water. Numerical computations by Hasselmann and Hasselmann (1981) of the full Bolzmann integral for water of arbitrary depth have shown that there is an approximate relation between transfer rates in deep water and water of finite depth: for a given frequency-direction spectrum, the transfer for finite depth is identical to the transfer for infinite depth, except for a scaling factor R:

$$S_{nl}(\text{finite depth}) = R(\bar{k}h) S_{nl}(\text{infinite depth}), \tag{3.59}$$

where $\bar{k}$ is the mean wave number. This scaling relation holds in the range $\bar{k}h > 1$, where the exact computations could be closely reproduced with the scaling factor

$$R(x) = 1 + \frac{5.5}{x}\left(1 - \frac{5x}{6}\right)\exp\left(-\frac{5x}{4}\right), \tag{3.60}$$

with $x = (3/4)\bar{k}h$. This approximation is used in the WAM model.

For constant frequency interval discretisation, Eq. (3.57) can be written as:

$$\begin{Bmatrix} \delta S_{nl} \\ \delta S_{nl+} \\ \delta S_{nl-} \end{Bmatrix} = \begin{Bmatrix} -2 \\ 1+\lambda \\ 1-\lambda \end{Bmatrix} \emptyset(f, E, E_+, E_-) \tag{3.61}$$

For logarithmic frequency discretisation, Eq. (3.57) becomes:

$$\begin{Bmatrix} \delta S_{nl} \\ \delta S_{nl+} \\ \delta S_{nl-} \end{Bmatrix} = \begin{Bmatrix} -2 \\ 1 \\ 1 \end{Bmatrix} \emptyset(f, E, E_+, E_-) \tag{3.62}$$

The contributions to the gradient terms $(\partial S_{nl} / \partial E)$ at the interacting wave numbers are obtained from:

$$\begin{Bmatrix} \delta(\partial S_{nl} / \partial E) \\ \delta(\partial S_{nl} / \partial E_+) \\ \delta(\partial S_{nl} / \partial E_-) \end{Bmatrix} = \begin{Bmatrix} -2\dfrac{\Delta f \Delta\theta}{\Delta f \Delta\theta} \cdot \dfrac{\partial \emptyset}{\partial E} \\ (1+\lambda)\dfrac{\Delta f \Delta\theta}{\Delta f_+ \Delta\theta} \cdot \dfrac{\partial \emptyset}{\partial E_+} \\ (1+\lambda)\dfrac{\Delta f \Delta\theta}{\Delta f_- \Delta\theta} \cdot \dfrac{\partial \emptyset}{\partial E_-} \end{Bmatrix} \tag{3.63}$$

As in Eq. (3.57), the total contribution to $\partial S_{nl} / \partial E$ at a given frequency f, and direction θ is found by summing the contributions from all frequencies, directions and the two configurations (primary and mirrored configuration).

Additional assumptions are required before computing Eq. (3.57) and Eq. (3.63) above. The reason for this is as follows: For the non-linear interactions, we always consider exchange of energy between the interacting wave numbers represented in frequency-direction space as: $(f, \theta), (f_+, \theta \pm \theta_3)$ and $(f_-, \theta \pm \theta_4)$. The frequencies f_+ and f_- are given by:

$$f_+ = (1+\lambda) f \tag{3.64}$$

$$f_- = (1-\lambda) f \tag{3.65}$$

where $\lambda = 0.25$. Now, our discretisation in frequency space needs to be finite: i.e. we discretise from a finite lower frequency, f_1 to a finite upper frequency, $f_{\max}$. Thus, there are problems with evaluating Eq. (3.57) and Eq. (3.63) at the two limits of the discretised frequency space. The question is what should be done when $f_+ > f_{\max}$ or $f_- < f_1$?

In order to answer this question, two additional assumptions are introduced:

Case 1: $f_+ > f_{\max}$

Firstly, the energy spectrum in the region $f > f_{\max}$ is assumed to follow a f^{-5} tail, since this is the diagnostic region. Secondly, in the vicinity of $f_{\max}$, there are contributions to S_{nl} from frequencies higher than the discretised maximum frequency in the model. The maximum frequency f_{upper}, which contributes energy into the discretised frequency range, can be found by solving:

$$f_{-} = (1-\lambda) f_{upper} = f_{\max} \tag{3.66}$$

or

$$f_{upper} = f_{\max} / (1-\lambda) \tag{3.67}$$

Thus, in order to correctly compute the contributions to S_{nl} in the vicinity of $f_{\max}$, the discretised frequency space is extended to f_{upper} and an f^{-5} tail assumed in this region.

Case 2: $f_{-} < f_1$

It is assumed that $E(f,\theta) = 0$ in the region $f < f_1$. This is a reasonable assumption if the discretised frequency space has been selected carefully to include all the energy containing frequencies.

Furthermore, since we assume $E = 0$ in the region $f < f_1$, the contributions from this region to the discretised frequency range is zero. In order to minimise the repetitive calculations involved in the computation of the non-linear source term a procedure is used, which consists of the following five steps:

1. For each discrete direction, θ, the indices in the direction array, to the right and left of $\theta \pm \theta_3, \theta \pm \theta_4$ are calculated and stored.

2. For each discrete frequency, f, in the extended frequency space, the indices to the right and left of $f_{+}[(1+\lambda) f]$ and $f_{-}[(1-\lambda) f]$ are calculated and stored.

3. For each discrete frequency, direction and configuration the spectral energy values $F(f_{+}, \theta \pm \theta_3), F(f_{-}, \theta \pm \theta_4)$ are found using bilinear interpolation. The values at the four corners of the $f-\theta$ grid are obtained from the indices obtained in steps (1) and (2) above.

4. The computed contributions to S_{nl} and $\partial S_{nl} / \partial E$ at $(f_{+}, \theta \pm \theta_3)$, and $(f_{-}, \theta \pm \theta_4)$ are distributed to the discrete frequency-direction mesh-points at the four corners of the $f-\theta$ grid.

5. The contributions to $\delta S_{nl}(f,\theta)$ and $\delta(\partial S_{nl} / \partial E)_{f,\theta}$ calculated from steps (3) and (4) are summed over all frequencies, directions and configurations to obtain $S_{nl}(f,\theta)$ and $(\partial S_{nl} / \partial F)_{f,\theta}$ at each $f-\theta$ mesh point.

3.3.3 Triad-wave interactions

In shallow water triad-wave interaction becomes important. Nonlinear transformation of irregular waves in shallow water involves the generation of bound sub- and super-harmonics and near-resonant triad interactions, where substantial cross-spectral energy transfer can take place in relatively short distance. The process of triad interactions exchanges energy between three interacting wave modes. The triad-wave interaction is modelled using the simplified approach proposed by Eldeberky and Battjes (1995, 1996).

$$S_{nl}(\sigma,\theta) = S_{nl+}(\sigma,\theta) + S_{nl-}(\sigma,\theta) \tag{3.68}$$

where

$$S_{nl+}(\sigma,\theta) = \max\begin{pmatrix} 0, \alpha_{EB} 2\pi c_g J^2 |\sin(\beta)| \left(cE^2(\sigma_-,\theta)\right) - \\ 2c_- E(\sigma_-,\theta) E(\sigma,\theta) \end{pmatrix} \tag{3.69}$$

$$S_{nl-}(\sigma,\theta) = -2S_{nl+}(\sigma_+,\theta) \tag{3.70}$$

This applies when $U_r > 0.1$ and $f(1) \leq 2.5\, f_{mean}$

Here $\sigma_- = \sigma/2$, $\sigma_+ = 2\sigma$, and $c_- = \sigma_-/k_-$ is the phase velocity, where k_- is the wave number corresponding to σ_-. α_{EB} is a tuning parameter. The biphase is parameterised by the parameter, β, which is given by

$$\beta = \frac{\pi}{2}\left(-1 + \tanh\left(\frac{0.2}{Ur}\right)\right) \tag{3.71}$$

The Ursell number, *Ur*, is given by

$$Ur = \frac{g}{2\sqrt{2}} \frac{H_{m0}}{\bar{\sigma}^2 d^2} \tag{3.72}$$

where $\bar{\sigma}$ is the mean angular frequency. The interaction coefficient, J, is given by

$$J = \frac{k_-^2\left(gd + 2c_-^2\right)}{-kd\left(gd + 2Bgd^3k^2 - \left(B + \frac{1}{3}\right)\sigma^2 d^2\right)} \tag{3.73}$$

where B=1/15.

3.3.4 Whitecapping

The mathematical development of a whitecap model can be traced to Hasselmann (1974). Assuming that the mechanism for whitecap dissipation is pressure induced decay, he obtained a dissipation source function that is linear in both the spectral density and the frequency

$$S_{ds} \approx -\omega E \tag{3.74}$$

Later, it was realised that other mechanisms are important. These mechanisms are the attenuation of short waves by the passage of large whitecaps and the extent of whitecap coverage (which depends on the overall steepness of the wave field). Combining these processes Komen et al. (1984) proposed a dissipation function formulated in terms of the mean frequency. This expression was reformulated by the WAMDI group (1988) in terms of wave number so as to be applicable in finite water depth

$$S_{ds} = -C'_{ds}\left(\frac{\hat{\alpha}}{\hat{\alpha}_{PM}}\right)^m \frac{k}{\bar{k}}\bar{\sigma}E \tag{3.75}$$

and C'_{ds} and m are fitting parameters, $\bar{\sigma}$ is the mean relative angular frequency, $\bar{k}$ is the mean wave number, $\hat{\alpha}$ is the overall steepness of the wave field and $\hat{\alpha}_{PM}$ is the value of $\hat{\alpha}$ for the Pierson-Moskowitz spectrum. The overall steepness is defined as

$$\hat{\alpha} = \bar{k}\sqrt{E_{tot}} \tag{3.76}$$

where E_{tot} is the total energy of energy spectrum and $\hat{\alpha}_{PM} = (3.02x10^{-3})^{1/2}$. In WAM cycle 3, $m = 4$ and $C'_{ds} = 2.36x10^{-5}$ (see also Komen et al., 1984 and WAMDI group,1988).

With the introduction of the Janssen's description for the wind input, it was realised (Janssen et al., 1989) that the dissipation source function needs to be adjusted in order to obtain a proper balance between wind input and dissipation at high frequencies. Thus, Eq. (3.75) was modified as (see Komen et al., 1994):

$$S_{ds}(f,\theta) = -C_{ds}\left(\frac{\hat{\alpha}}{\hat{\alpha}_{PM}}\right)^m \left\{(1-\delta)\frac{k}{\bar{k}} + \delta\left(\frac{k}{\bar{k}}\right)^2\right\}\bar{\sigma}E(f,\theta) \tag{3.77}$$

C_{ds}, δ and m are constants. In WAM cycle 4 the values for C_{ds}, δ and m are respectively, 4.1x10^{-5}, 0.5 and 4. In the present implementation the tunable constants are $C^*_{ds} = C_{ds}/(\alpha_{PM})^4$ and δ while m = 4. The default values for C^*_{ds} and δ are respectively, 4.5 and 0.5.

The formulation of the source term due to whitecapping is as standard applied over the entire spectrum and the integral wave parameters used in the formulation is calculated based on the whole energy spectrum

$$\bar{\sigma} = 2\pi\bar{f} = 2\pi\left(\frac{\int_0^{2\pi}\int_0^{\infty} E(f,\theta) f^{p_\sigma} df d\theta}{\int_0^{2\pi}\int_0^{\infty} E(f,\theta) df d\theta}\right)^{p_\sigma} \tag{3.78}$$

$$\sqrt{\bar{k}} = \left(\frac{\int_0^{2\pi} \int_0^{\infty} E(f,\theta) \left(\sqrt{k}\right)^{p_k} df d\theta}{\int_0^{2\pi} \int_0^{\infty} E(f,\theta) df d\theta} \right)^{p_k} \tag{3.79}$$

where $p_\sigma = p_k = -1$ is applied. The integrals are calculated by a split into a resolved part (prognostic region) and unresolved part (deterministic region) following the approach used in Appendix A. For wave conditions with a combination of wind-sea and swell this may results in too strong decay of energy on the swell components. Introducing a separation of wind-sea and swell, the predictions for these cases can be improved by excluding the dissipation on the swell part of the spectrum and by calculating the wave parameters, used in the formulation of whitecapping, from the wind-sea part of the spectrum. The separation of wind-sea and swell are estimated using the definitions in Section 5.1.

To improve the the whitecapping for wave conditions with a combination of wind-sea and swell Bidlot et. al 2007 proposed a revised formulation of whitecapping. Here Eq. (3.77) is still applied but the mean relative angular frequency and the mean wave number are calculated using Eq. (3.78) and Eq. (3.79), respectively, with $p_\sigma = p_k = 1$ and the default values for C_{ds}^* and δ are changed to 2.1 and 0.6, respectively.

3.3.5 Bottom friction

The rate of dissipation due to bottom friction is given by

$$S_{bot}(f,\theta) = -(C_f + f_c(\overline{u} \cdot \overline{k})/k) \frac{k}{\sinh 2kd} E(f,\theta) \tag{3.80}$$

where C_f is a friction coefficient, k is the wave number, d is water depth, f_c is the friction coefficient the for current and u is the current velocity. The coefficient C_f is typically 0.001-0.01 m/s depending on the bed and flow conditions (Komen et al., 1994). The default value for f_c is 0 corresponding to excluding the effect of the current on the bottom friction.

Four models for determination of the possibilities for the dissipation coefficient are implemented:

1. A constant friction coefficient C_f. Tests with regional versions of the WAM model (see Chapter IV in Komen et al., 1994) have shown that the mean JONSWAP value of C_f = 2*0.038/g = 0.0077 m/s is adequate for moderate storms. The default value for C_f is 0.0077 m/s.

2. A constant friction factor f_w in which the friction coefficient is calculated as

$$C_f = f_w u_b \tag{3.81}$$

where u_b is the rms wave orbital velocity at the bottom given by

$$u_b = \left[2 \int_{f_1}^{f_{max}} \int_{\theta} \frac{\bar{\sigma}^2}{\sinh^2(kh)} E(f,\theta) d\theta df \right]^{1/2} \quad (3.82)$$

The default value for f_w is 0.015*$2^{1/2}$ = 0.021.

3. A constant geometric roughness size k_N, as suggested by Weber (1991) in which the friction coefficient is calculated by Eq. (3.81) and the friction factor is calculated using the expression of Jonsson and Carlsen, 1966

$$\begin{aligned} f_w &= e^{-5.977+5.213(a_b/k_N)^{-0.194}} && a_b/k_N >= 2.016389 \\ f_w &= 0.24 && a_b/k_N < 2.016389 \end{aligned} \quad (3.83)$$

Here a_b is the orbital displacement at the bottom given by

$$a_b = \left[2 \int_{f_1}^{f_{max}} \int_{\theta} \frac{1}{\sinh^2(kh)} E(f,\theta) d\theta df \right]^{1/2} \quad (3.84)$$

The default value for k_N is 0.04 m. This value was suggested by Weber, 1991 as being compatible with the flow conditions for a range of swell and wind sea spectra.

4. A constant median sediment size D_{50}, in which the bed is modelled as a mobile bed. This approach was first used in a third generation wind-wave model by Tolman (1996). However, the present implementation is very different from Tolman's formulation. Instead of using the Grant and Madsen model for determining ripple dimensions (as used by Tolman), we use the empirical expressions of Nielsen (1979) which is based on field measurements. Thereafter, the bed roughness is calculated using the expression by Swart (1976). Finally, the friction coefficient is computed as the product of the wave friction factor (using the expression of Jonsson and Carlsen, 1966) and the bottom orbital velocity. The default value for D_{50} is 0.00025 m.

Details of the bottom friction formulation can be found in Johnson and Kofoed-Hansen (2000).

3.3.6 Wave breaking

Depth-induced breaking (or surf breaking) occurs when waves propagate into very shallow areas, and the wave height can no longer be supported by the water depth. The formulation of wave breaking derived by Battjes and Janssen (1978) is used. The source term is written as (Eldeberky and Battjes, 1996):

$$S_{surf}(f,\theta) = -\frac{2\,\alpha_{BJ}\,Q_b\,\bar{f}}{X} E(f,\theta) \quad (3.85)$$

where $\alpha_{BJ} \approx 1.0$ is a calibration constant, Q_b is the fraction of breaking waves, $\bar{f}$ is the mean frequency and X is the ratio of the total energy in the random wave train to the energy in a wave train with the maximum possible wave height

$$X = \frac{E_{tot}}{(H_m^2/8)} = \left(\frac{H_{rms}}{H_m}\right)^2 \tag{3.86}$$

where E_{tot} are the total wave energy, H_m is the maximum wave, and $H_{rms} = \sqrt{8E_{tot}}$.

In shallow water at a local water depth, d, the maximum wave height can be calculated from

$$H_m = \gamma d \tag{3.87}$$

where γ is the breaker parameter. The value of γ varies from 0.5 to 1.0 depending on the beach slope and wave parameters.

When the waves are described using the directionally decoupled parametric formulation, the maximum wave height is influenced by the wave steepness as well.

$$H_m = \gamma_{ws} \cdot \tanh\left(k_{mean} \cdot d \cdot \frac{\gamma}{\gamma_{ws}}\right) / k_{mean} \tag{3.88}$$

Where γ_{ws} is the breaking parameter related to breaking due to wave steepness and γ is the breaking parameter related to wave breaking due to water depth. k_{mean} is the mean wave number.

The default values for the tunable variables α_{BJ} , γ and γ_{ws} are respectively 1.0, 0.8 and 1.0.

In a random wave train with a truncated Raleigh distribution of wave heights the fraction of breaking waves Q_b is determined from

$$\frac{Q_b - 1}{\ln Q_b} = X = \left(\frac{H_{rms}}{H_m}\right)^2 \quad \Leftrightarrow \quad Q_b = \exp\left(\frac{-(1-Q_b)}{(H_{rms}/H_m)^2}\right) \tag{3.89}$$

Q_b is obtained solving the nonlinear Eq. (3.89) using a Newton-Raphson iteration. As initial guess for the nonlinear iteration is used the following explicit approximation to Q_b (Hersbach, 1996 private communication)

$$\begin{aligned} Q_b &= (1+2x^2)\exp(-1/x) && && x < 0.5 \\ &= 1-(2.04z)(1-0.44z); && z = 1-x; && 0.5 \le x < 1 \\ &= 1 && && x \ge 1 \end{aligned} \tag{3.90}$$

Based on laboratory data and field data it has been shown that the breaking parameter γ varies significantly depending on the wave conditions and the bathymetry. Kaminsky and Kraus (1993) found that γ values in the range between 0.6 and 1.59 with an average of

0.79. A number of expressions for determination of the breaking parameter γ have been proposed in literature. Battjes and Stive (1985) found that g depends weakly on the deep water wave steepness. They proposed the following expression

$$\gamma = 0.5 + 0.4 \tanh(33 s_0) \tag{3.91}$$

Here $s_0 = H_0 / L_0$ is the deep water steepness, where H_0 and L_0 is the wave height and the wave length, respectively, in deep water. This formulation cannot be used in the present spectral wave model, because the value of γ is not determined based on local parameters. Nelson (1987, 1994) found that γ can be determined as a function of the local bottom slope, $\partial d / d\partial s$, in the mean wave direction. Nelson suggested the following expression

$$\begin{aligned} \gamma &= 0.55 + 0.88 \exp\left(-0.012 \operatorname{cotan}\left(\frac{\partial d}{\partial s} \right) \right) && d \le 100 \\ \gamma &= 0.55 && d > 100 \end{aligned} \tag{3.92}$$

Recently, Ruessink et al. (2003) have presented a new empirical form for γ, where γ is determined as a function of the product of the local wave number k and the water depth d

$$\gamma = 0.76 kd + 0.29 \tag{3.93}$$

Ruessink et al. showed that using this formulation for the breaking parameter the prediction of the wave heights in the breaking zone can be improved for barred beaches. However, the new formulation is also applicable to planar beaches.

3.4 Diffraction

Diffraction can be modelled using the phase-decoupled refraction-diffraction approximation proposed by Holthuijsen et al. (2003).

The approximation is based on the mild-slope equation for refraction and diffraction, omitting phase information. In the presence of diffraction the magnitude of the wave number, k, (the gradient of the phase function of a harmonic wave) is given by

$$k^2 = \kappa^2 \left(1 + \delta_a \right) \tag{3.94}$$

where κ is the separation parameter determined from linear wave theory and δ_a is a diffraction parameter defined by

$$\delta_a = \frac{\nabla \cdot (c c_g \nabla a)}{\kappa^2 c c_g a} \tag{3.95}$$

Here c and c_g are the phase velocity and group velocity, respectively, without diffraction effects and a is the wave amplitude. Now the phase velocity, C, and the group velocity, C_g, in the presence of diffraction are given by

$$C = \frac{\sigma}{k} = \frac{\sigma}{\kappa} \frac{\kappa}{k} = \frac{c}{\sqrt{1 + \delta_a}} \tag{3.96}$$

$$C_g = c_g \frac{k}{\kappa} = c_g \sqrt{1+\delta_a} \tag{3.97}$$

For wave propagation over slowly varying depths and currents the diffraction-corrected propagation velocities $(C_x, C_y, C_\sigma, C_\theta)$ of a wave group in the four-dimensional phase space $\vec{x}$, σ and θ are given by

$$(C_x, C_y) = \vec{C}_g + \vec{U} = \vec{c}_g(1+\delta_a) + \vec{U} \tag{3.98}$$

$$C_\sigma = \frac{\partial \sigma}{\partial d}\left[\frac{\partial d}{\partial t} + \vec{U}\cdot\nabla_{\vec{x}} d\right] - C_g \vec{\kappa}\cdot\frac{\partial \vec{U}}{\partial s} \tag{3.99}$$

$$C_\theta = -\left[\left(\left(\frac{\sqrt{1+\delta_a}}{\kappa}\frac{\partial \sigma}{\partial d}\frac{\partial d}{\partial m}\right) - \frac{C_g}{2(1+\delta_a)}\frac{\partial \delta_a}{\partial m}\right) + \frac{\vec{\kappa}}{\kappa}\cdot\frac{\partial \vec{U}}{\partial m}\right] \tag{3.100}$$

Following the approach by Holthuijsen et al. (2003) the wave amplitude is replaced by the square root of the directional integrated spectral energy density

$$A(o) = \sqrt{\int_0^{2\pi} E(\sigma,\theta)\, d\theta} \tag{3.101}$$

4 Numerical Implementation

4.1 Space Discretisation

The discretisation in geographical and spectral space is performed using a cell-centred finite volume method. In the geographical domain, an unstructured mesh is used. The spatial domain is discretised by subdivision of the continuum into non-overlapping elements. The elements can be of arbitrarily shaped polygons, however, in this paper only triangles are considered. The action density, $N(\vec{x}, \sigma, \theta)$ is represented as a piecewise constant over the elements and stored at the geometric centres. In frequency space, a logarithmic discretisation is used

$$\sigma_1 = \sigma_{\min} \qquad \sigma_l = f_\sigma \sigma_{l-1} \qquad \Delta\sigma_l = \sigma_{l+1} - \sigma_{l-1} \qquad l = 2, N_\sigma \tag{4.1}$$

where f_σ is a given factor, σ_{min} is the minimum discrete angular frequency and N_σ is the number of discrete frequencies. In the directional space, an equidistant discretisation is used

$$\theta_m = (m-1)\Delta\theta \qquad \Delta\theta_m = 2\pi / N_\theta \qquad m = 1, N_\theta \tag{4.2}$$

where N_θ is the number of discrete directions. The action density is represented as piecewise constant over the discrete intervals, $\Delta\sigma_l$ and $\Delta\theta_m$, in the frequency and directional space.

Integrating Eq. (3.7) over area A_i of the ith element, the frequency increment $\Delta\sigma_l$ and the directional increment $\Delta\theta_m$ give

$$\frac{\partial}{\partial t}\int_{\Delta\theta_m}\int_{\Delta\sigma_l}\int_{A_i} N d\Omega d\sigma d\theta - \int_{\Delta\theta_m}\int_{\Delta\sigma_l}\int_{A_i} \frac{S}{\sigma} d\Omega d\sigma d\theta = \int_{\Delta\theta_m}\int_{\Delta\sigma_l}\int_{A_i} \nabla\cdot(\bar{F}) d\Omega d\sigma d\theta \tag{4.3}$$

where Ω is an integration variable defined on A_i and $\bar{F} = (F_x, F_y, F_\sigma, F_\theta) = \bar{v}N$ is the convective flux. The volume integrals on the left-hand side of Eq. (4.3) are approximated by one-point quadrature rule. Using the divergence theorem, the volume integral on the right-hand can be replaced by integral over the boundary of the volume in the $\bar{x}$, σ, θ-space and these integrals are evaluated using a mid-point quadrature rule. Hence, Eq. (4.3) can be written

$$\frac{\partial N_{i,l,m}}{\partial t} = -\frac{1}{A_i}\left[\sum_{p=1}^{NE}(F_n)_{p,l,m}\Delta l_p\right] - \frac{1}{\Delta\sigma_l}\left[(F_\sigma)_{i,l+1/2,m} - (F_\sigma)_{i,l-1/2,m}\right] - \frac{1}{\Delta\theta_m}\left[(F_\theta)_{i,l,m+1/2} - (F_\theta)_{i,l,m-1/2}\right] + \frac{S_{i,l,m}}{\sigma_l} \tag{4.4}$$

where NE is the total number of edges in the cell (NE = 3 for triangles). $(F_n)_{p,l,m} = \left(F_x n_x + F_y n_y\right)_{p,l,m}$ is the normal flux through the edge *p* in the geographical space with length Δl_p. $\vec{n} = (n_x, n_y)$ is the outward pointing unit normal vector of the boundary in the geographical space. $(F_\sigma)_{i,l+1/2,m}$ and $(F_\theta)_{i,l,m+1/2}$ are the flux through the face in the frequency and directional space, respectively.

Convective flux in geographical space

The convective flux in geographical space is derived using either a first-order upwinding scheme or a higher-order scheme. The convective flux at the edge between element i and j is given by is given by

$$F_n = c_n N_{face} = c_n \left(\frac{1}{2}(N_l + N_r) - \frac{1}{2}\frac{c_n}{|c_n|}(N_l - N_r) \right) \tag{4.5}$$

Where N_l and N_r is the action density the left and the right of the edge and c_n is the propagation speed normal to the cell face

$$c_n = \frac{1}{2}\left(\vec{c}_i + \vec{c}_j\right) \cdot \vec{n} \tag{4.6}$$

Using the first-order scheme N_l and N_r is approximated by the cell-centred values N_i and N_j, respectively.

The numerical diffusion introduced using first-order upwinding schemes can be significant, see e.g. Tolman (1991, 1992). In small-scale coastal applications and application dominated by local wind, the accuracy obtained using these schemes are considered to be sufficient. However, for the case of swell propagation over long distances, higher-order upwinding schemes may have to be applied.

Second-order spatial accuracy is achieved by employing a linear gradient-reconstruction technique for calculating the values N_l and N_r. The gradients are calculated based on cell-centred values. To provide stability and minimise oscillatory effects, an ENO (Essentially Non-Oscillatory) type procedure is applied to limit the gradients. Additionally, a simple limiter is applied for N_{face} at the interface in that this value is limited by N_l, N_r, N_i and N_j.

Convective flux in frequency and directional space

The convective flux in frequency and directional space is derived using a first-order upwinding scheme.

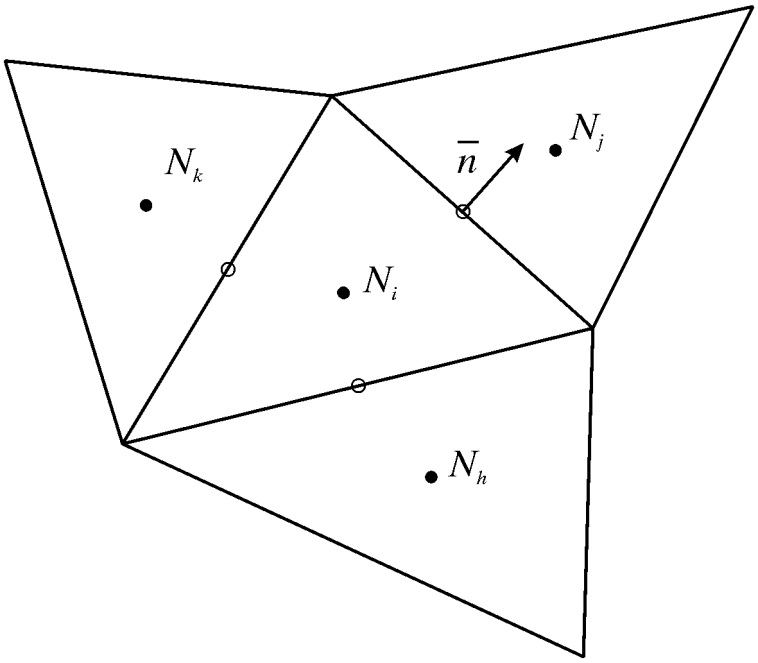

Figure 4.1 ● centroid point and ○ midpoint of edges

4.2 Time Integration

The integration in time is based on a fractional step approach. Firstly, a propagation step is performed calculating an approximate solution N^* at the new time level (n+1) by solving Eq. (3.7) without the source terms. Secondly, a source terms step is performed calculating the new solution N^{n+1} from the estimated solution taking into account only the effect of the source terms.

Propagation step

The propagation step is carried out by an explicit Euler scheme

$$N^*_{i,l,m} = N^n_{i,l,m} + \Delta t \left(\frac{\partial N_{i,l,m}}{\partial t} \right)^n \tag{4.7}$$

where $\left(\partial N_{i,l,m} / \partial t\right)^n$ is given by Eq. (4.4) with $S_{i,l,m} = 0$ and Δt is the global time step.

To overcome the severe stability restriction, a multi-sequence integration scheme is employed following the idea by Vilsmeier and Hänel (1995). Here, the maximum time step is increased by locally employing a sequence of integration steps, where the number of steps may vary from element to element. Using the explicit Euler scheme, the time step is limited by the CFL condition stated as

$$Cr_{i,l,m} = \left| c_x \frac{\Delta t}{\Delta x_i} \right| + \left| c_y \frac{\Delta t}{\Delta y_i} \right| + \left| c_\sigma \frac{\Delta t}{\Delta \sigma_l} \right| + \left| c_\theta \frac{\Delta t}{\Delta \theta_m} \right| < 1 \tag{4.8}$$

where $Cr_{j,l,m}$ is the Courant number and Δx_i and Δy_i are characteristic length scale in the x and y-directions for the ith element. The maximum local Courant number, $Cr_{max,\,i}$, is determined for each element in the geographical space, and the maximum local time step, $\Delta t_{\max,i}$, for the ith element is then given by

$$\Delta t_{\max,i} = \Delta t / Cr_{\max,i} \tag{4.9}$$

To ensure accuracy in time, the intermediate levels have to be synchronised. Therefore, the fraction, f_g, of the local time step to the global time step is chosen as powers of ½

$$f_g = \left(\frac{1}{2}\right)^{g-1}, \qquad g = 1, 2, 3, \ldots \tag{4.10}$$

The local time step, Δt_i, is then determined as the time step with the maximum value of the level index, g, for which

$$\Delta t_i \, f_g < \Delta t_{\max,i} \tag{4.11}$$

Two neighbouring elements are not allowed to have an index difference greater than one. The edges get the lowest index of the two elements they support.

The calculation is performed using a group concept, in that groups of elements are identified by their index, *g.* The computational speed-up using the multi-sequence integration compared to the standard Euler method increases with increasing number of groups. However, to get accurate results in time, the maximum number of groups must be limited. In the present work, the maximum number of levels is 32.

Source term step

The source term step is performed using an implicit method

$$N_{i,l,m}^{n+1} = N_{i,l,m}^{*} + \Delta t \left[\frac{(1-\alpha) S_{i,l,m}^{*} + \alpha S_{i,l,m}^{n+1}}{\sigma_l} \right] \tag{4.12}$$

where α is a weighting coefficient that determines the type of finite difference method. Using a Taylor series to approximate S^{n+1} and assuming the off-diagonal terms in the functional derivative $\partial S / \partial E$ to be negligible such that the diagonal part $\partial S_{i,l,m} / \partial E_{i,l,m} = \gamma$, Eq. (4.12) can be simplified as

$$N_{i,l,m}^{n+1} = N_{i,l,m}^{n} + \frac{(S_{i,l,m}^{*} / \sigma_l)\Delta t}{(1 - \alpha\gamma\Delta t)} \tag{4.13}$$

For growing waves ($\gamma > 0$), an explicit forward difference is used ($\alpha = 0$), while for decaying waves ($\gamma < 0$), an implicit backward difference ($\alpha = 1$) is applied.

Especially for small fetches, stability problems may occur. Hence, a limiter on the maximum increment of spectral energy between two successive time steps is introduced. The limiter proposed by Hersbach and Janssen (1999) is applied

$$\Delta N_{\max} = \frac{3\times 10^{-7}}{(2\pi)^3} g\tilde{u}_* \sigma_l^{-4} \sigma_{\max} \Delta t \tag{4.14}$$

where σ_{max} is the maximum discrete frequency and $\tilde{u}_*$ u defined by

$$\tilde{u}_* = \max(u_*, (\sigma_{PM} / \sigma)) \tag{4.15}$$

Here u_* is the wind friction speed.

4.3 Boundary Conditions

At the land boundaries in the geographical space, a fully absorbing boundary condition is applied. The incoming flux components (the flux components for which the propagation velocity normal to the cell face is positive) are set to zero. No boundary condition is needed for the outgoing flux components. At an open boundary, the incoming flux is needed. Hence, the energy spectrum has to be specified at an open boundary. In the frequency space, the boundaries are fully absorbing. No boundary conditions are needed in the directional space.

4.4 Diffraction

For instationary calculations the inclusion of diffraction can cause oscillations in the numerical solution in areas with very fine resolution and/or large ratio between element sizes. For quasi-stationary calculations the inclusion of diffraction can cause convergence problems. To reduce these problems a smoothing is introduced for the discrete values of the square root of the directional spectral energy density, $A_{i,l} = A(x_i, y_i, \sigma_l)$, which is used in the calculation of the diffraction parameter. This smoothing is done according to

$$A_{i,l}^k = (1-\alpha) A_{i,l}^{k-1} + \alpha \left(A_{i,l}^{k-1} \right)^* \qquad k = 1, nsteps \tag{4.16}$$

Here *k* is the number of smoothing steps and *α* is the smoothing factor. The smooth approximation, A^* , is calculated by first calculating the vertex values using the pseudo-Laplacian procedure proposed by Holmes and Connell (1989) and then calculating the cell-centred values by averaging the vertex values corresponding to each element. By default one filtering step is performed with a smoothing factor of α=1. Note, the smoothing is only used in the calculation of the diffraction parameter. Increasing the smoothing (increasing the number of smoothing steps) with reduce the oscillation/convergence problem, but will also has the effect that the diffraction effect will be reduced.

4.5 Structures

The horizontal dimension of structures, such as piers and offshore wind turbines, is usually much smaller than the resolution used in the computational grid. Therefore, the presence of these structures must be modelled by a subgrid scaling technique. Two approaches have been developed for taking into account the effect of point structures. The effects of the structures can be taken into account by introducing a decay term to

reduce the wave energy behind the structure. This formulation is only accurate when the energy decay is limited and the reflection of the wave energy is not taken into account. The second approach is based on a correction of the convective flux term in geographical space.

4.5.1 Source term approach

The discrete source term, $S_{i,l,m} = S(\vec{x}_i, \sigma_l, \theta_m)$, due to the effect of a point structure can be written

$$S_{i,l,m} = -\frac{c}{A_i} c_g E_{i,l,m} \tag{4.17}$$

where A_i is the area of the cell i in the mesh in which the structure is located, c is the reflection factor, c_g is the group celerity and $E_{i,l,m} = E(\vec{x}_i, \sigma_l, \theta_m)$ is the energy density. The reflection factor determines the amount of energy, which hits the structure, there is reflected. For a circular cylinder the factor c is obtained as

$$c = D \cdot r \tag{4.18}$$

where $0 \le r \le 1$ is the reflection coefficient and D is the diameter of the structure. The reflection coefficient r is obtained from a pre-defined table. Alternatively, the factor c can be specified directly as a function of the water depth and the wave period using a user-defined table.

The pre-defined table consist of the reflection factors, $r_{i,j}$, as function of discrete values of the dimensionless diameter, $\tilde{D}$, and the dimensionless wave period, $\tilde{T}$

$$\begin{aligned} \tilde{D}_i &= \tilde{D}_{min} + (i-1)\frac{\tilde{D}_{max} - \tilde{D}_{min}}{nd - 1} \qquad i = 1, nd \\ \tilde{T}_i &= \tilde{T}_{min} + (j-1)\frac{\tilde{T}_{max} - \tilde{T}_{min}}{nt - 1} \qquad j = 1, nt \end{aligned} \tag{4.19}$$

where

$$\begin{aligned} \tilde{D} &= \frac{D}{d} \\ \tilde{T} &= \frac{2\pi}{\sigma}\sqrt{\frac{g}{d}} \end{aligned} \tag{4.20}$$

Here where *d* is the water depth, *g* is the acceleration of gravity, nd=18 is the number of discrete diameters, $\tilde{D}_{min}$=0.2 is the minimum dimensionless diameter, $\tilde{D}_{max}$=7 is the maximum dimensionless diameter, nt=20 is the number of discrete wave periods, $\tilde{T}_{min}$=1.566 is the minimum dimensionless wave period, $\tilde{T}_{max}$=31.321 is the maximum dimensionless wave period. The reflection factor at a given location is calculated from the table using bilinear interpolation.

The user-defined table containing the reflection factor as function of the water depth and the wave period must be given in form of an ASCII file. The first part of the ASCII file must contains the header information. The header information consists of two lines each with three space separated items. The first line contains the number of discrete depth, nd, the minimum depth (in m), d_{min}, and the maximum depth (in m), d_{max}. The second line contains the number of discrete wave periods, nt, the minimum wave period (in s), T_{min}, and the maximum wave period (in s), T_{max}. Data follows after the header information. The data consist of the reflection factors, $c_{i,j}$, as function of discrete values of the depth and wave period

$$d_i = d_{min} + (i-1)\frac{d_{max} - d_{min}}{nd - 1} \qquad i = 1, nd$$
$$t_j = t_{min} + (j-1)\frac{t_{max} - t_{min}}{nt - 1} \qquad j = 1, nt \tag{4.21}$$

The format of a reflection factor table is shown below

nd d_{min} d_{max}
nt T_{min} T_{max}
$c_{1,1}$ $c_{1,2}$ $c_{1,3}$ … $c_{1,nt}$
$c_{2,1}$ $c_{2,2}$ $c_{2,3}$ … $c_{2,nt}$
…
…
$c_{nd,1}$ $c_{nd,2}$ $c_{nd,3}$ … $c_{nd,nt}$

The reflection factors in the file must be space separated. The reflection factor at a given location is calculated from the table using bilinear interpolation.

In spherical coordinates the area A_i should be replaced by $\widehat{A_i} = A_i R^2 cos\phi$, where A_i is the area of the cell in the spherical coordinate system, *R* is the radius of the earth and ϕ is the latitude.

4.5.2 Convective flux approach

The contribution to the time-derivative of the cell-centred value of the wave action density, $N_{i,l,m} = N(\vec{x}_i, \sigma_l, \theta_m)$, from the convective transport in the geographical space into the element *i* is given by

$$-\frac{1}{A_i}\sum_{p=1}^{NE}(F_n)_{p,l,m}\Delta l_p \tag{4.22}$$

where A_i is the area of the cell, *NE* is the total number of edges in the cell (*NE*=3 for triangles and *NE*=4 for quadrilateral elements), $(F_n)_{p,l,m} = \left(F_x n_x + F_y n_y\right)_{p,l,m}$ is the normal flux through the edge *p* in the geographical space with length Δl_p and $\vec{n} = \left(n_x, n_y\right)$ is the outward pointing unit normal vector of the boundary in the geographical space.

The convective flux in geographical space is derived using a first-order upwinding. The convective flux at the edge between cell *i* and the neighbouring cell *j* is given by

$$F_n = c_n\left(\frac{1}{2}(N_i + N_j) - \frac{1}{2}\frac{c_n}{|c_n|}(N_i - N_j)\right) \tag{4.23}$$

where N_i and N_j are cell-centred values of the action density and c_n is the propagation speed normal to the cell face

$$c_n = \frac{1}{2}(\vec{c}_i + \vec{c}_j)\cdot\vec{n} \tag{4.24}$$

To take into account the effect of the structures a correction of the normal flux is introduced

$$(F_n)^*_{p,l,m} = (F_n)_{p,l,m} - (\Delta F_n)_{p,l,m} \tag{4.25}$$

where the correction term is given by

$$\begin{aligned} (\Delta F_n)_{p,l,m} &= \frac{c}{\Delta l_p}(F_n)_{p,l,m} \qquad (F_n)_{p,l,m} < 0 \\ (\Delta F_n)_{p,l,m} &= 0 \qquad\qquad\quad (F_n)_{p,l,m} \geq 0 \end{aligned} \tag{4.26}$$

Hence, the decay of the energy in the cell *i* due to the point structure can be taken into account by adding the following correction term to the time-derivative of the cell-centred value of the wave action density

$$\frac{1}{A_i}\sum_{p=1}^{NE}(\Delta F_n)_{p,l,m}\Delta l_p \tag{4.27}$$

The reflection factor, *c*, is obtained as described in the previous section. To include the reflected energy the following term is subtracted from the time-derivative of the cell-centred value of the wave action density for the neighbouring cell *j*

$$\frac{1}{A_j}(\Delta F_n)_{p,l,m+\Delta m}\Delta l_p \tag{4.28}$$

It is assumed that the energy is reflected 180 degrees. Hence, $\theta_{m+\Delta m} = \theta_m + \pi$. If $\theta_{m+\Delta m}$ do not correspond to a discrete direction, a weighted correction is added to the two neighbouring discrete directions.

In spherical coordinates the length Δl_p in the correction term should be replaced by

$$\widehat{\Delta l_p} = \Delta l_p R\sqrt{n_\lambda n_\lambda + n_\phi n_\phi cos\phi cos\phi} \tag{4.29}$$

where Δl_p and (n_λ, n_ϕ) are the length and the outward pointing unit normal vector in the spherical coordinate system.

5 Output Data

5.1 Field Type

The following types of output data is possible

- Parameters
  - Integral wave parameters
  - Input parameters
  - Model parameters
- Spectral parameter (directional spectrum):
  The direction energy/action spectrum is obtained by integration over the discretised frequencies
- Spectral parameter (frequency spectrum):
  The frequency energy/action spectrum is obtained by integration over the discretised directions
- Spectral parameter (directional-frequency spectrum):
  The direction energy/action spectrum is obtained by integration over the discretised frequencies

Integral Wave Parameters

The integral wave parameters can be calculated for the total spectrum, for the wind sea part of the spectrum and the swell part of the spectrum. The distinction between the wind sea and the swell can be estimated in three different ways.

Constant threshold frequency

Swell wave components are defined as those components fulfilling the following criterion

$$f < f_{threshold} \quad or \quad \cos(\theta - \theta_w) < 0 \tag{5.1}$$

where θ and θ_w is the wave propagation and wind direction, respectively. $f_{threshold}$ is the constant threshold frequency, which must be specified by the user. The default value is 0.125 Hz (~$T_{threshold}$ = 8 s).

Dynamic threshold frequency (version 1)

Swell wave components are defined as those components fulfilling the following criterion

$$f < f_{threshold} \quad or \quad \cos(\theta - \theta_w) < 0 \tag{5.2}$$

where θ and θ_w is the wave propagation and wind direction, respectively. $f_{threshold}$ is the dynamic threshold frequency defined by

$$f_{threshold} = 0.7 f_{p,PM} \left(\frac{E_{PM}}{E_{\mathrm{mod}\,el}} \right)^{0.31} \tag{5.3}$$

where $f_{p,PM}$ is the peak frequency for a fully developed wind-sea described by a Pierson-Moskowitz spectrum (see also Young (1999) p. 92) given by

$$f_{p,PM} = 0.14 \frac{g}{U_{10}} \tag{5.4}$$

E_{PM} is the total wave energy in a fully developed wind-sea described by a Pierson-Moskowitz spectrum

$$E_{PM} = \left(\frac{U_{10}}{1.4g} \right)^4 \tag{5.5}$$

and E_{total} is the calculated total wave energy for the components (also named the wind sea components) fulfilling the following criterion

$$f > 0.8 \cdot f_{p,PM} \; and \; \cos(\theta - \theta_w) > 0 \tag{5.6}$$

Dynamic threshold frequency (version 2)

Swell wave components are defined as those components fulfilling the following wave-age based criterion

$$\frac{U_{10}}{c} \cos(\theta - \theta_w) < 0.83 \tag{5.7}$$

where U_{10} is the wind speed, c the phase speed and θ and θ_w is the wave propagation and wind direction, respectively.

The integral wave parameters are given by

1. Significant wave height, H_{m0} (m)

$$H_{mo} = 4\sqrt{m_o} \tag{5.8}$$

2. Maximum wave height, H_{max} (m)

The maximum wave height, H_{max} (m) is estimated as

$$H_{max} = min(H^1_{max}, H^2_{max}) \tag{5.9}$$

$H^1_{\max}$ is determined assuming Rayleigh distributed waves

$$H^1_{\max} = H_{m0}\sqrt{\frac{1}{2}\ln N} \tag{5.10}$$

where N is the number of waves estimated as N = *duration*/T_{01}. The duration is set to 3 hours (10800 s).

$H^2_{\max}$ is determined assuming monochromatic waves

$$H^2_{\max} = d\frac{0.141063\alpha + 0.0095721\alpha^2 + 0.0077829\alpha^3}{1 + 0.0788340\alpha + 0.0317567\alpha^2 + 0.0093407\alpha^3} \tag{5.11}$$

where $\alpha = \frac{L}{d} = \frac{2\pi}{kd}$, where k is the wave number corresponding to the peak wave period and d is the water depth.

3. Peak period, Tp (s)

$$T_p = 1/f_p \tag{5.12}$$

The peak frequency f_p is calculated from the one-dimensional frequency spectrum using a parabolic fit around the discrete peak.

The scheme for computing the peak frequency can be formulated thus:

- Search through 1D frequency spectrum and obtain the index, i_p corresponding to maximum spectral density.
- Using $f_0 = f(i_p - 1)$, $f_1 = f(i_p)$, $f_2 = f(i_p + 1)$ and similarly for E_0, E_1, E_2, the peak frequency is given by

$$f_p = f(i_p - 1) - \frac{b}{2c} \tag{5.13}$$

where

$$b = \frac{(f_2 - f_0)^2(E_1 - E_0) - (f_1 - f_0)^2(E_2 - E_0)}{(f_1 - f_0)(f_2 - f_0)^2 - (f_1 - f_0)^2(f_2 - f_0)} \tag{5.14}$$

$$c = \frac{(f_1 - f_0)\ (E_2 - E_0) - (f_2 - f_0)\ (E_1 - E_0)}{(f_1 - f_0)\ (f_2 - f_0)^2 - (f_1 - f_0)^2 (f_2 - f_0)} \tag{5.15}$$

4. Mean period, T01 (s)

$$T_{01} = m_0 / m_1 \tag{5.16}$$

5. Zero crossing period, T02 (s)

$$T_{02} = \sqrt{m_0 / m_2} \tag{5.17}$$

6. Energy averaged mean period, T-10 (s)

$$T_{-10} = 1/\bar{f} = m_{-1} / m_0 \tag{5.18}$$

7. Peak wave direction, θ_p (degree)

   This is defined as the discrete direction with maximum energy.

8. Mean wave direction, $\bar{\theta}$ (degree)

$$\bar{\theta} = 270 - \tan^{-1}(b/a) \tag{5.19}$$

where

$$a = \frac{1}{m_0} \int_0^{2\pi} \int_0^{\infty} \cos\left(\frac{3}{2}\pi - \theta\right) E(f,\theta)\, df\, d\theta$$

$$b = \frac{1}{m_0} \int_0^{2\pi} \int_0^{\infty} \sin\left(\frac{3}{2}\pi - \theta\right) E(f,\theta)\, df\, d\theta \tag{5.20}$$

9. Directional standard deviation, σ (degree)

$$\sigma = \left[2\left(1 - \left(a^2 + b^2\right)^{1/2}\right)\right]^{1/2} \cdot 180/\pi \tag{5.21}$$

10. Wave velocity components

$$(u, v) = (H_{m0} \cos(270 - \theta_m), H_{m0} \sin(270 - \theta_m)) \tag{5.22}$$

11. Radiation stresses, S_{xx}, S_{xy} and S_{yy} (m3/s2)

$$S_{xx} = \frac{1}{2} g\left(f_{u2} + f_{pp}\right)$$
$$S_{xy} = \frac{1}{2} g\left(f_{uv}\right) \qquad (5.23)$$
$$S_{yy} = \frac{1}{2} g\left(f_{v2} + f_{pp}\right)$$

where

$$f_{pp} = \int_0^{2\pi}\int_0^{\infty}\left(1+\frac{2kd}{\sinh(2kd)}\right)E(f,\theta)\,df\,d\theta$$

$$f_{u2} = \int_0^{2\pi}\int_0^{\infty}\cos^2\left(\frac{3}{2}\pi-\theta\right)\left(1+\frac{2kd}{\sinh(2kd)}\right)E(f,\theta)\,df\,d\theta \qquad (5.24)$$

$$f_{uv} = \int_0^{2\pi}\int_0^{\infty}\cos\left(\frac{3}{2}\pi-\theta\right)\sin\left(\frac{3}{2}\pi-\theta\right)\left(1+\frac{2kd}{\sinh(2kd)}\right)E(f,\theta)\,df\,d\theta$$

$$f_{v2} = \int_0^{2\pi}\int_0^{\infty}\sin^2\left(\frac{3}{2}\pi-\theta\right)\left(1+\frac{2kd}{\sinh(2kd)}\right)E(f,\theta)\,df\,d\theta$$

12. Particle velocities

The calculation of the horizontal and vertical particle velocity components *u* and *w* is based on Stokes first order theory for progressive waves, see e.g. Dean and Dalrymple (1991) p79f:

$$u(z,\phi) = \tfrac{1}{2}\omega H\frac{\cosh k(z+d)}{\sinh kh}\cos\phi$$
$$w(z,\phi) = \tfrac{1}{2}\omega H\frac{\sinh k(z+d)}{\sinh kh}\sin\phi \qquad (5.25)$$

where ω is the cyclic angular frequency, *H* is wave height, *k* the wave number, *d* water depth, *z* vertical coordinate and ϕ the phase of the wave.

Using the directionally decoupled parametric formulation the root-mean-squared of the maximum value of two components can be calculated as

$$u_{\max}(z) = \sqrt{\int_0^{2\pi} (2\omega \frac{\cosh k(z+d)}{\sinh kh})^2 E(\theta) d\theta}$$

$$w_{\max}(z) = \sqrt{\int_0^{2\pi} (2\omega \frac{\sinh k(z+d)}{\sinh kh})^2 E(\theta) d\theta} \quad (5.26)$$

where $E(\theta)$ is the wave energy at wave direction θ.

Using the fully spectral formulation the root-mean-squared of the maximum value of two components can be calculated as

$$u_{\max}(z) = \sqrt{\int_0^{2\pi} \int_0^{\infty} (2\omega \frac{\cosh k(z+d)}{\sinh kh})^2 E(f,\theta) df d\theta}$$

$$w_{\max}(z) = \sqrt{\int_0^{2\pi} \int_0^{\infty} (2\omega \frac{\sinh k(z+d)}{\sinh kh})^2 E(f,\theta) df d\theta} \quad (5.27)$$

where $E(f,\theta)$ is the wave energy at wave direction θ.

The following values are included in the output:

- Maximum horizontal particle wave velocity at the sea bottom, $U_{max}(z= -d)$
- Maximum horizontal particle wave velocity at the free surface, $U_{max}(z= 0)$
- Maximum vertical particle wave velocity at the free surface, $W_{max}(z= 0)$
- Maximum horizontal particle wave velocity at a level z_0, $U_{max}(z= z_0)$
- Maximum vertical particle wave velocity at a level, z_0, $W_{max}(z= z_0)$

z_0 is defined by

$$z_0 = d + \Delta d \quad (5.28)$$

where Δd is a user-specified distance above the bed.

13. Wave power

The energy transport for a harmonic wave is $P_{energy} = \rho g c_g E$ in magnitude, where E is the energy density and c_g is the group velocity, ρ is the density of water and g is the acceleration of gravity. In random seas the following to definitions of the wave power can be used

- Omni-directional wave power (energy sink) P_{energy}

$$P_{Energy} = \rho g \int_0^{2\pi} \int_0^{\infty} c_g(f,\theta) E(f,\theta) df d\theta \tag{5.29}$$

- Directional wave power (energy transport) $\vec{P}_{Energy} = (P_{energy,x}, P_{energy,y})$

$$\vec{P}_{Energy} = \rho g \int_0^{2\pi} \int_0^{\infty} \vec{c}_g(f,\theta) E(f,\theta) df d\theta$$

$$P_{Energy,x} = \rho g \int_0^{2\pi} \int_0^{\infty} c_g(f,\theta) \cos(\theta) E(f,\theta) df d\theta \tag{5.30}$$

$$P_{Energy,y} = \rho g \int_0^{2\pi} \int_0^{\infty} c_g(f,\theta) \sin(\theta) E(f,\theta) df d\theta$$

Input Wave Parameters

The following input parameters can be written

- Water levels, (m)
- Water depth, D (m)
- Current velocity, U (m/s)
- Wind speed, U10 (m/s)
- Wind direction, θ_w (degree)
- Ice concentration

Model Wave Parameters

The following model parameters can be written

- Friction coefficient (m^2/s)
- Breaking parameter, gamma
- CFL number
- Time levels
- Length (m)
- Area (m^2)
- Threshold period (s)
- Wind friction speed (m/s)
- Roughness length
- Drag coefficient

- Charnock coefficient

Spectral Parameters

- Wave energy
- Wave action

5.2 Output Format

The following types of output formats is possible

- Point series
  - Selected field data in geographical defined points
  - The geographical coordinates are either taken from the dialog or from an ASCII file
- Lines series
  - Selected field data in geographical defined lines
  - The geographical coordinates are either taken from the dialog or from an ASCII file
- Area series
  - Selected field data in geographical defined area
- The geographical coordinates of the area are specified in the dialog

6 References

/1/ Battjes, J.A. and J.P.F.M. Janssen, (1978), Energy loss and set-up due to breaking of random waves, *Proc. 16th Int. Conf. Coastal Eng.,* ASCE, pp 569-587.

/2/ Battjes, J.A. and M.J.F. Stive, (1985), Calibration and verification of a dispersion model for random breaking waves, *Geophys. Res*., **90**, 9159-9167.

/3/ Dean, R G and R A Dalrymple (1991), Water wave mechanics for engineers and scientists. *World Scientific Publishing Co*., Pte. Ltd.

/4/ Eldeberky, Y. and J.A. Battjes. (1995), Parameterization of triad interactions in wave energy models, paper presented at Coastal Dynamics Conference, ASCE., Gdansk, Poland.

/5/ Eldeberky, Y. and J.A. Battjes, (1996), Spectral modelling of wave breaking: Application to Boussinesq equations, *J. Geophys. Res.*, **101, No. C1**, 1253-1264.

/6/ Fenton, J.D. (1990), Nonlinear wave theories, in B. LeMéhauté & D.M. Hanes, eds, *The Sea-Ocean Engineering Science*, Part A, Vol. **9**, Wiley, New York, pp. 3-25.

/7/ Hasselmann, K., 1962: On the nonlinear energy transfer in a gravity-wave spectrum, Part 1, General theory. *J. Fluid Mech.*, **12**, 481-500.

/8/ Hasselmann K., (1974), On the spectral dissipation of ocean waves due to whitecapping, *Bound. Layer Meteor.*, **6**, 107-127.

/9/ Hasselmann, S., K. Hasselmann, (1981), A symmetrical method for computing the nonlinear transfer in a gravity-wave spectrum, *Hamburger Geophys. Einzelschr.*, Serie A., 52,8.

/10/ Hasselmann, S., K. Hasselmann, 1985), Computation and parameterizations of Non-linear Energy Transfer in a Gravity-wave Spectrum, Part 1: A New Method for Efficient Computations of the exact Non-linear Transfer Integral, *J. Phys. Oceanog.*, **15**, 1369-1377.

/11/ Hasselmann, S., K. Hasselmann, K., J.H. Allender and T. P. Barnett (1985), Computation and parameterizations of Non-linear Energy Transfer in a Gravity-wave Spectrum, Part 2: Parameterisations of non-linear energy transfer for applications in wave models, *J. Phys. Oceanog.*, **15**, 1378-1391.

/12/ Hersbach, H. and P. A. E. M. Janssen, (1999), Improvement of short-fetch behaviour in the wave ocean model, *J. Atmos. & Ocean Tech*., **16**, 884-892.

/13/ Holthuijsen, L.H, Booij, N. and Herbers, T.H.C., (1989) A Prediction Model for Stationary, Short-crested Waves in Shallow Water with Ambient Currents, *Coastal Engineering*, **13**, 23-54.

/14/ Holthuijsen, L.H, A. Herman and N. Booij (2003), Phase-decoupled refraction-diffraction for spectral wave models, *Coastal Engineering*, **49**, 291-305.

/15/ Homes D.G. and Connell S.D. (1989), Solution of the 2D Navier-Stokes equations on unstructured grids, *J. Comput. Phys*., 155, 54-74.

/16/ Janssen, P.A.E.M., (1989), Wave induced stress and the drag of airflow over sea waves, *J. Phys. Oceanogr*., **19**, 745-754.

/17/ Janssen P.A.E.M., Lionello, P and Zambresky L. (1989), On the interaction of wind and waves, *Phil. Trans. R. Soc. Lond*., **A 329**, 289-301.

/18/ Janssen, P.A.E.M., (1991), Quasi-linear theory of wind wave generation applied to wave forecasting, *J. Phys. Oceanogr*., **21**, 1631-1642.

/19/ Johnson H.K., and H. Kofoed-Hansen, (2000), Influence of Bottom friction on sea roughness and its impact on shallow water wind wave modelling, *J. Phys. Oceanogr*., **30**, 1743-1756.

/20/ Jonsson, I.G., (1966), Wave boundary layers and friction factors, *Proc. 10th Int. Conf. Coastal Eng.,* Tokyo, ASCE, pp 127-148.

/21/ Kaminsky, G.M. and N.C. Kraus, (1993), Evaluation of depth-limited wave breaking criteria, *Proc. Of 2nd Int. Symposium on Ocean Wave Measurement and Analysis*, New Orleans, 180-193.

/22/ Komen G.J., S. Hasselman and K. Hasselman (1984), On the existence of a fully developed wind-sea spectrum, *J. Phys. Oceanogr*., **14**, 1271-1285.

/23/ Komen, G.J., L. Cavaleri, M. Doneland, K. Hasselmann, S. Hasselmann and P.A.E.M. Janssen, (1994), Dynamics and modelling of ocean waves. Cambrigde University Press, UK, 560pp.

/24/ Nelson, R.C., (1987), Design wave heights on very mild slopes: An experimental study, *Civil. Eng. Trans*., *Inst. Eng*., Aust., **29**, 157-161.

/25/ Nelson, R.C., (1994) Depth limited wave heights in very flat regions, *Coastal Eng*., **23**, 43-59.

/26/ Nielsen, P., (1979), Some basic concepts of wave sediment transport, *Series paper 20* Institute of Hydrodynamic and Hydraulic Engineering, Technical University of Denmark, 160 pp.

/27/ Ris, R.C. (1997) Spectral modelling of wind waves in coastal areas, PhD. thesis, Delft 1997.

/28/ Ruessink, B.G., D.J.R. Walstra, and H.N. Southgate, (2003), Calibration and verification of a parametric wave model on barred beaches, *Coastal Eng*., **48**, 139-149.

/29/ Smith, S.D. and E.G. Banke, (1975) Variation of the sea surface drag coefficient with wind speed. *Quart. J. Roy. Meteor. Soc,* **101**, 665-673.

/30/ Snyder, R.L., F.W. Dobson, J.A. Elliott and R.B. Long, (1981), Array measurements of atmospheric pressure fluctuations above surface gravity waves, *J. Fluid Mech*., **102**, 1-59.

/31/ Swart D.H., (1976), Predictive equations regarding coastal transports. *Proc 15th Conf Coastal Engng,* 2, pp. 1113–1132.

/32/ Tolman, H.L., (1991), A third generation model for wind waves on slowly varying, unsteady and inhomogeneous depths and currents, *J. Phys. Oceanogr*., **21**, 782-797.

/33/ Tolmann, H.L. (1992), Effects of numerics on the physics in a third-generation wind-wave model, *J. Phys. Oceanogr*, **22**, 1095-1111.

/34/ Tolman, H.L. and D. Chalikov, (1996), Source terms in a third-generation wind-wave model. *J. Phys. Oceanogr.*, **26**, 2497-2518.

/35/ Vilsmeier R. and D. Hänel, (1995), Adaptive solutions for unsteady laminar flows on unstructured grids, *Int. J. Numer. Meth. Fluids*., Vol. 22, 85-101.

/36/ Young I.R., (1999), Wind generated ocean waves, In Elsevier Ocean Engineering Book Series, Volume 2. Eds. R. Bhattacharyya and M.E. McCormick, Elsevier.

/37/ WAMDI-group: S. Hasselmann, K. Hasselmann, E. Bauer, P.A.E.M. Janssen, G.J. Komen, L. Bertotti, P. Lionello, A. Guillaume, V.C. Cardone, J.A. Greenwood, M. Reistad, L. Zambresky and J.A. Ewing, (1988) 'The WAM model - a third generation ocean wave prediction model', *J. Phys. Oceanogr.*, **18**, 1775-1810.

/38/ Weber, S.L, (1991), Bottom friction for wind sea and swell in extreme depth-limited situations, *J. Phys. Oceanogr*., **10**, 1712-1733.

/39/ Wu, J., (1982) Wind-stress coefficients over sea surface from breeze to huricane, *J. Geophys. Res..,* **87**, 9704-9706.

6.1 Other Relevant References

/40/ Astrup, P., N.O. Jensen and T. Mikkelsen, 1996: Surface roughness model for LINCOM. Risø-R-900 (EN), 30pp.

/41/ Atatürk, S.S and K.B. Katsaros, 1999: Wind stress and surface waves observed on Lake Washington. *J. Phys. Oceanogr.,* **29**, 633-650.

/42/ Barthelmie, R.J., M.S. Courtny, J. Højstrup, and P. Sanderhoff, 1994. The Vindeby Project: A Description, *Report Risø-R-741 (EN),* Risø National Laboratory, Roskilde, Denmark.

/43/ Barthelmie, R.J., M.S. Courtney, B. Lange, M. Nielsen and A.M. Sempreviva (1999a): Offshore wind resources at Danish measurement sites. *Proc. European wind energy conference,* Nice, France 1999.1101-1104.

/44/ Barthelmie, R.J., B. Lange and M.Nielsen (1999b): Wind resources at Rødsand and Omø Stålgrunde. Risø internal report Risø-I-1456(EN).

/45/ Benoit, M., F. Marcos and F. Becq, 1996: Development of a third-generation shallow-water wave model with unstructured spatial meshing. *Proc. 25th Int. Conf. on Coastal Engrg*, ASCE, Orlando, 465-487.

/46/ Bidlot, J., P. Janssen, and S. Abdalla, 2007: A revised formulation of ocean wave dissipation and its model impact. Technical Report Memorandum 509, ECMWF, Reading, U. K.

/47/ Booij, N., R. C. Ris and L. H. Holthuijsen, (1999), A third-generation wave model for coastal regions. 1. Model description and validation. *J. Geophys. Res*., **104**, 7649-7666.

/48/ Bouws, E. and G.J. Komen, 1983: On the balance between growth and dissipation in an extreme, depth-limited wind-sea in the southern North Sea. *J. Phys. Oceanogr*., **13**, 1653-1658.

/49/ Bourassa, M.A., D.G. Vincent and W.L. Wood, 1999: A flux parameterization including the effects of capillary waves and sea state. *J. Phys. Oceanogr*., **56**, 1123-1138.

/50/ Charnock, H., 1955: Wind Stress on a water surface. *Quart. J. Roy. Meteorol. Soc.,* **81**, 639-640.

/51/ Collins, J.I., 1972: Prediction of shallow water spectra. *J. Geophys. Res*., **77**, 2693-2707.

/52/ Donelan, M. A., J. Hamilton and W. H. Hui, 1985: Directional Spectra of Wind-Generated Waves. *Phil. Trans. R. Soc. Lond*., **A 315**, 509-562.

/53/ Donelan, M.A., 1990: Air-Sea Interaction. *The Sea,* B. LeMehaute and D. Hanes (Eds.), John Wiley and Sons, 239-292.

/54/ Donelan, M.A., F.W. Dobson, S.D. Smith and R.J. Anderson, 1993: On the dependence of sea surface roughness on wave development. *J. Phys. Oceanogr.*, **23**, 2143-2149.

/55/ Donelan, M.A., W.M. Drennan, and K. B. Katsaros, 1997: The air-sea momentum flux in conditions of wind sea and swell. *J. Phys. Oceanogr*., **15**, 2087-2099.

/56/ Frank, H.P. and L. Landberg, 1997: Modelling the wind climate of Ireland. *Boundary-Layer Meteorol.,* **85**, 359-378.

/57/ Geernaert, G.L., S.E. Larsen, and F. Hansen, 1987: Measurements of the wind stress, heat flux and turbulence intensity during storm conditions over the North Sea. *J. Geophys. Res*., **92C**, 13,127 - 13,139.

/58/ Geernaert, G.L., K.B. Katsaros and K. Richter, 1986: Variation of the drag coefficient and its dependency on sea state. *J. Geophys. Res*., **91C,** 6, 7667-7669.

/59/ Garratt, J.R., 1977: Review of drag coefficients over oceans and continents, *Monthly Weather Review,* **105**, 915.

/60/ Günther, H., S. Hasselmann and P.A.E.M. Janssen, 1992: The WAM model cycle 4. DKRZ Technical Report No 4, Hamburg.

/61/ Gulev, S.K. and L. Hasse, 1998: North Atlantic wind waves and wind stress fields from voluntary observing ship data. *J. Phys. Oceanogr*., **28**, 1107-1130.

/62/ Hansen, C. and Larsen, S.E., 1997: Further work on the Kitaigorodskii roughness length model: A new derivation using Lettau's expression on steep waves. *Geophysica,* **33** (2)*,* 29-44.

/63/ Hasselmann, K., T.P. Barnett, E. Bouws, H. Carlson, D.E. Cartwright, K. Enke, J.A. Wing, H. Gienapp, D.E. Hasselmann, P. Kruseman, A. Meerburg, P. Müller, D.J. Olbers, K. Ricter, W. Sell and H. Walden, 1973: Measurements of wind-wave growth and swell decay during the Joint North Sea Wave Project (JONSWAP). Dtsch. Hydrogr. Z. Suppl. A (12), 95 pp.

/64/ Hersbach, H., 1997: 'Application of the adjoint of the WAM model to inverse wave modelling', *J. Geophys. Res.,* **103**, C5, 10469-10487.

/65/ Jackson, P.S. and J.C.R. Hunt, 1975: Turbulent wind flow over a low hill. *Quart. Journal of the Royal Meteorological Society*, **101**, 929-955.

/66/ Janssen, J.A.M., 1997: Does wind stress depend on sea-state or not? – A statistical error analsysis of HEXMAX data. *Boundary-Layer Meteorology,* **83**, 479-503.

/67/ Janssen, P.A.E.M., 1992: Experimental evidence of the effect of surface waves on the airflow. *J. Phys. Oceanogr.*, **22**, 1600-1604.

/68/ Janssen P.A.E.M. and Günther, (1992), Consequences of the effect of surface gravity waves on the mean air flow, *Int. Union of Theor. and Appl. Mech. (IUTAM)*, Sydney, Australia, 193-198.

/69/ Janssen, P.A.E.M., 1998: On the effect of ocean waves on the kinetic energy balance and consequences for the initial dissipation technique. *J. Phys. Oceanogr.*, **29**, 530-534.

/70/ Johnson H.K., and H. Kofoed-Hansen, (1998), MIKE 21 OSW3G - Technical documentation, Internal Rep., Danish Hydraulic Institute.

/71/ Johnson, H.K., J. Højstrup, H.J. Vested and S.E. Larsen, 1998: On the Dependence of Sea Surface Roughness on Wind Waves. *J. Phys. Oceanogr.,* **28,** 1702-1716.

/72/ Johnson, H.K., H.J. Vested, H. Hersbach, J. Højstrup, and S.E. Larsen, 1999: 'On the coupling between wind and waves in the WAM model', *Journal of Atmospheric and Oceanic Technology, Vol 16, No. 11, 1780-1790.*

/73/ Jonsson I.G. and N.A. Carlsen, (1976), Experimental and theoretical investigations in an oscillatory turbulent boundary layer, *J. Hydraul. Res*., **14**, 45-60.

/74/ Kahma, K.K. and C.J. Calkoen, 1994: Growth curve observations, *In Dynamics and Modelling of Ocean Waves by Komen et al,* Cambridge University Press, 174-182.

/75/ Katsaros, K. B, M.A. Donelan and W.M. Drennan, 1993: Flux measurements from a SWATH ship in SWADE. *J. Mar. Sys.,* **4**, 117-132.

/76/ Kitaigorodskii, S.A., 1970: The physics of air-sea interaction. Translated for Russian by A. Baruch, Israel Program for Scientific Translations, Jerusalem, 237pp.

/77/ Kitaigorodskii, S.A., 1998: The dissipation subrange in wind wave spectra. *Geophysica*, **34** (3), 179-207.

/78/ Kofoed-Hansen, H; and J.H. Rasmussen, 1998*:* Modelling of non-linear shoaling based on stochastic evolution equations. *Coastal Engineering,* **33**, 203-232.

/79/ Komen, G.J., P.A.E.M. Janssen, V. Makin, K. Mastenbroek and W. Oost, 1998: Review: On the sea state dependence of the Charnock parameter, *J. Glob Atmos. Ocean System,* **5**, 367-388.

/80/ Kudryatsev, V.N. and V.K. Makin (1996): Transformation of wind in the coastal zone. KNMI, Scientific Report WR 96-04.

/81/ Large, W.G. and S. Pond, 1981: Open ocean momentum flux measurements in moderate to strong winds. *J. Phys. Oceanogr.,* **14,** 464-482.

/82/ Lettau, H., 1969: Note on areodynamic roughness-parameter estimation on basis of roughness element distribution. *J. Appl. Meteor.,* **8**, 820-832.

/83/ Makin V.K. and V.N. Kudryatsev, 1999: Coupled sea surface-atmosphere model. 1. Wind over waves coupling. *J. Geophys. Res.,* **104C**, 7613-7623.

/84/ Makin V.K., V.N. Kudryatsev and C. Mastenbroek, 1995: Drag of the sea surface. *Boundary-Layer Meteorol.,* **73**, 159-182.

/85/ Mastenbroek, C., G.J.H. Burgers, P.A.E.M. Janssen, 1993: The dynamical coupling of a wave model and a storm surge model through the atmospheric boundary layer. *J. Phys. Oceanogr.,* **23**, 1856-1866.

/86/ Merzi, N. and W.H. Graf, 1985: Evaluation of the drag coefficient considering the effects of mobility of the roughness elements. *Ann. Geophys.,* **3**, 473-478.

/87/ Monbaliu, J., 1994: On the use of the Donelan wave spectral parameter as a measure for the measure for the roughness of wind waves. *Boundary-Layer Meteorol*, **67**, 277-291.

/88/ Nordeng, T.E., 1991: On the wave age dependent drag coefficient and roughness length at sea. *J. Geophys. Res.,* **96**, 7167-7174.

/89/ Oost, W.A., 1998: The Knmi HEXMAX stress data – a reanalysis. *Boundary-Layer Meteorology,* **86**, 447-468.

/90/ Perrie, W. and B. Toulany 1990: Fetch relations for wind-generated waves as a function of wind-stress scaling, *J. Phys. Oceanogr.*, **20**, 1666-1681.

/91/ Phillips, O.M., 1960: On the dynamics of unsteady gravity waves of finite amplitude, Part 1. *J. Fluid Mech.,* **9**, 193-217.

/92/ Phillips, O.M., 1981: The structure of short gravity waves on the ocean surface. In: *Spaceborn Synthetic Aperture Radars for Oceanography*, the Johns Hopkins Press.

/93/ Rasmussen, J.H. (1999): Deterministic and stochastic modelling of surface gravity waves in finite water depth. *Ph.D. thesis*, Department of Hydrodynamic and Water Resources (ISVA), Technical University of Denmark.

/94/ Resio, D.T., B. Tracy, C.L. Vincent, and J.H. Rasmussen (1999): Non-linear energy fluxes and the finite-depth equilibrium range in wave spectra. *Submitted to J. Phys. Oceanogr.*

/95/ Ris, R.C., L.H. Holthuijsen and N. Booij, 1999: A third-generation wave model for coastal regions. 2. Verification. *J. Geophys. Res*., **104C**, 7667-7681.

/96/ Smith, S.D., 1988: Coefficients for sea surface wind stress, heat flux and wind profiles as function of wind speed and temperature. *J. Geophys. Res*., **93C**, 15,467 - 15,472.

/97/ Smith, S.D. 1980: Wind stress and heat flux over the open ocean in gale force winds. *J. Phys. Oceanogr.,***10**, 709-726.

/98/ Smith, S.D., R.J.Anderson, W.A. Oost, C. Kraan, N. Maat, J. DeCosmo, K.B. Katsaros, K.L. Davidson, K. Bumke, L.Hasse, and H.M. Chadwick, 1992: 'Sea surface wind stress and drag coefficients: The HEXOS results. *Boundary-Layer Meteorology,* **60**, 109-142.

/99/ Smith, S.D., Katsaros, K.B., Oost, W.A. and Mestayer, P., 1996: The impact of the HEXOS Programme. *Boundary-Layer Meteorol.*, **78**, 109-142.

/100/ Schneggenburger, C., 1998: Spectral wave modelling with nonlinear dissipation. *Phd. dissertation*, GKSS-Forschungszentrum Geesthacht GmbH. 117pp.

/101/ Taylor, P.A. and R.J. Lee, 1984: *Simple guidelines for estimating wind speed variations due to small-scale topographic features*, Climatol Bull, 18, 3-32.

/102/ Troen, I. and E.L. Petersen, 1989: *European Wind Atlas*, Risø National Laboratory. 656pp.

/103/ Toba, Y., N. Iida, H. Kawamura, N. Ebuchi and I.S.F. Jones, 1990: Wave dependence on sea-surface wind stress. *J. Phys. Oceanogr.,* **20**, 705-721.

/104/ Vledder, van G.P., Ronde, de J.G. and Stive, M.J.F. (1994), Performance of a spectral wind-wave model in shallow water, *Proc. 24th Int. Conf. Coastal Eng.*, ASCE, pp 761-774.

/105/ Vledder, G. van, 1999: Source term investigation in SWAN. Report prepared for Rijkswaterstaat, the Netherlands, by Alkyon, the Netherlands. Report A162.

/106/ Weber, S.L., 1991: Bottom friction for wind sea and swell in extreme depth-limited situations, *J. Phys. Oceanogr.,* **21**, 149-172.

/107/ Wu, J., 1980: Wind stress coefficients over sea surface near neutral conditions. A revisit, *J. Phys. Oceanogr.,* **10**, 727-740.

/108/ Yelland, M. and P.T. Taylor, 1996: Wind stress measurements from the open ocean. *J. Phys. Oceanogr.,* **26**, 1712-1733.

/109/ Yelland, M., B.I. Moat, P.K. Taylor, R.W. Pascal, J. Hutchings and V.C. Cornell, 1998: Wind stress measurements from the open ocean corrected for airflow distortion by the ship. *J. Phys. Oceanogr.,* **28**, 1511-1526.

/110/ Taylor, P.K. and M.J. Yelland, 1999: The dependence of sea surface roughness on the height and steepness of the waves. Manuscript submitted to. *J. Phys. Oceanography,* July 1999.

/111/ Young, I. and L.A. Verhagen, 1996: 'The growth of fetch-limited waves in water of finite depth. Part I and II.', *Coastal Engineering,* **29** pp.47-99.

/112/ Young, I. and R.M. Gorman, 1995: 'Measurements of the evolution of ocean wave spectra due to bottom friction', *J. Geophys. Res*, **100**, C6, pp.10987-11004.

APPENDICES

APPENDIX A

Spectral Wave Parameters

A Spectral Wave Parameters

The spectral wave parameters the total energy, E_{tot}, the mean angular frequency, $\bar{\sigma}$, and the mean wave number, $\bar{k}$, are calculated as follows

$$E_{tot} = m_0 \tag{A.1}$$

$$\bar{\sigma} = 2\pi\bar{f} = 2\pi\frac{m_o}{m_{-1}} \tag{A.2}$$

$$\sqrt{\bar{k}} = \frac{m_o}{I} \tag{A.3}$$

The spectral moments used in the calculation of spectral wave parameters are computed as follows

$$m_i = \int_0^{2\pi}\int_0^{\infty} E(f,\theta) f^i df d\theta \tag{A.4}$$

Split Eq. (A.4) into resolved part and unresolved part

$$m_i = m_{i_1} + m_{i_2} \tag{A.5}$$

$$m_{i1} = \int_0^{2\pi}\int_0^{f_{\max}} E(f,\theta) f^i df d\theta \tag{A.6}$$

$$m_{i_2} = \int_0^{2\pi}\int_{f_{\max}}^{\infty} E(f,\theta) f^i df d\theta \tag{A.7}$$

Therefore:

$$m_{i_2} = \int_{f_{\max}}^{\infty} \underbrace{\left[\int_0^{2\pi} E(f_{\max},\theta)\ d\theta\right]}_{I_{\max}} \left(\frac{f}{f_{\max}}\right)^{-5} \cdot f^i df = I_{\max}\frac{f_{\max}^{1+i}}{4-i} \tag{A.8}$$

Eq. (A.8) above is not valid for $i = 4$. Finally, m_i is given by:

$$m_i = \int_0^{2\pi}\int_0^{f_{\max}} E(f,\theta) f^i df d\theta + \frac{f_{\max}^{1+i}}{4-i}\left[\int_0^{2\pi} E(f_{\max},\theta) d\theta\right] \tag{A.9}$$

Finally, *I* used in the calculation of the mean wave number is given by

$$I = \int_{f_1}^{f_{max}} \int_{\theta} E(f,\theta) \frac{df d\theta}{\sqrt{k}} + \int_{f_{max}}^{\infty} \int_{\theta} E(f_{max},\theta) \left(\frac{f}{f_{max}} \right)^{-5} \frac{df d\theta}{\sqrt{k}}$$

$$= \int_{f_1}^{f_{max}} \int_{\theta} E(f,\theta) \frac{df d\theta}{\sqrt{k}} + \int_{\theta} \frac{\sqrt{g}}{10\pi} E(f_{max},\theta) d\theta \qquad \text{(A.10)}$$

where the deep water expression for k has been used in the second term on the RHS of Eq. (A.10).